

**TARGETING TUMOR MICROENVIRONMENT TO  
IMPROVE IMMUNOTHERAPY RESPONSES**

by

**Sultan Damgacı Ertürk**

B.S., in Physics, Istanbul University, 2011

M.Sc., in Nuclear Physics, Istanbul University, 2014

Submitted to the Institute of Biomedical Engineering  
in partial fulfillment of the requirements  
for the degree of  
Doctor  
of  
Philosophy

Boğaziçi University

2020

**TARGETING TUMOR MICROENVIRONMENT TO  
IMPROVE IMMUNOTHERAPY RESPONSES**

**APPROVED BY:**

Assoc. Prof. Dr. Albert Güveniş .....  
(Thesis Advisor)

Prof. Dr. Robert J. Gillies .....  
(Thesis Co-advisor)

Prof. Dr. Cengizhan Öztürk .....

Assist. Prof. Dr. Bora Garipcan .....

Assoc. Prof. Dr. Natarajan Raghunand .....

Assoc. Prof. Dr. David L. Morse .....

**DATE OF APPROVAL:** 19 December 2019



*I dedicated this thesis to my beautiful mom, Zeliha. The reason of what I become today.*

## ACKNOWLEDGMENTS

Undertaking this PhD has been truly a life-changing experience for me and I am thankful to many people for turning these long years into an unforgettable experience for me.

First, I would like to express my special appreciation to my advisor, Assoc. Prof. Dr. Albert Güveniş for supporting and guiding me to complete this study. In particular, it was tough to adjust myself during my switch from Physics to Biomedical Engineering Department and then join to Moffitt Cancer Center. I would not temp to do those without his encouragement and support.

I will forever be thankful to my co-supervisor, Prof. Dr. Robert J. Gillies. He gave me the chance to lead an industry collaboration as soon as I joined to Moffitt Cancer Center, regardless of my very limited experience with his endless belief and support. I would give him the most credit for becoming the kind of scientist I am today. I will never forget how I started to this journey and how he taught me to walk through all of those obstacles with an unbelievable patience.

My special words of thanks should also go to my committee members Prof. Dr. Cengizhan Öztürk, Assist. Prof. Dr. Bora Garipcan, Assoc. Prof. Dr. Raghunand Natarajan and Assoc. Prof. Dr. David Morse for their time, and scientific advices.

I have never walked alone during those years. I have had privilege to both receive excessive amount of support from high level of scientists and become their friends in Dr. Gillies' Lab during my studies. They were the ones, who actually made those dreams possible for my thesis study. No words can express my appreciation to them. Thank you Drs Arig Ibrahim- Hashim, Smitha Pillai, Pedro Enriquez Navas, William Dominguez Viqueira, Gary Martinez, Dominique Abrahams, and Epi Ruiz for involving in to all of my experiments and for your invaluable contributions.

I would like to also thank to my lab mates and friends Drs Shonagh Russell, Veronica Estrealla, Bruna Perassi, Mehdi Damaghi, Nika Fedorchuk, Stanislav Andieiev, Narges Tafreshi and Nella Delva for their continued support and never leaving me alone while I was starting my new life in United States.

I would like to also thank to my friend, also classmate & colleague, Özge Can Kaplan, for her support and help to format my thesis based on institute requirements.

I gratefully acknowledge the funding and intellectual support from H. Lee Moffitt Cancer Center and Helix Biopharma. In particular, I am also grateful to Dr Marni Uger (Helix Biopharma), for sharing her extensive knowledge with me and teaching how to design & develop experiments, data analysis and reporting.

I owe a lot to my parents Zeliha & Mustafa Damgacı, my brother and sister in law Fatih & Havvanur Damgacı who encouraged and helped me at every stage of my personal and academic life, and longed to see this achievement come true. Last but not least, Bilge, my little baby niece, thank you for being in this world, smiling and giving me continued hope whenever I look at to your face. Your presence is my inspiration.

## ACADEMIC ETHICS AND INTEGRITY STATEMENT

I, Sultan Damgacı Ertürk, hereby certify that I am aware of the Academic Ethics and Integrity Policy issued by the Council of Higher Education (YÖK) and I fully acknowledge all the consequences due to its violation by plagiarism or any other way.

Name :

---

Signature:

---

Date:

---

## ABSTRACT

### TARGETING TUMOR MICROENVIRONMENT TO IMPROVE IMMUNOTHERAPY RESPONSES

The acidic microenvironment of solid tumors has suppressing effects on immune cells, accordingly immunotherapy responses. This thesis composed of two main studies as measuring tumor pH with non-invasive methods using MRI/MRSI and targeting tumor acidity to improve immunotherapy responses.

Firstly, we developed two different MR imaging techniques to monitor tumor pH. We have shown that the difference in pHs before and after L-DOS47 treatments were statistically significantly different than control mice. To our knowledge this is the first study demonstrates the neutralization ability of proposed drug in in-vivo models.

The second aim of this dissertation was to develop combinatorial approaches have potential to be used in the clinic for patient benefits. This includes neutralization of tumor acidity in order to improve immunotherapy responses with L-DOS47 currently in clinical trials and well tolerated. We have demonstrated in-vivo that L-DOS47 treatment is effective to promote survival when combined with anti-PD1.

Overall, under the scope of this study we were able to develop two imaging techniques with MRI to monitor tumor pH and elaborated a combinatorial treatment model in order to boost immunotherapy responses. Isovue, L-DOS47 and anti-PD1 are already approved by FDA to be used in the clinic which makes this study remarkable for a new clinical trial design.

**Keywords:** Tumor microenvironment, Cancer, Immunotherapy, MR Imaging.

## ÖZET

### İMMÜNÖTREAPİYİ GELİŞTİRMEK İÇİN TÜMÖR METABOLİZMASINI HEDEFLEME

Katı tümörlerin asidik mikroçevresi immün hücreleri ve buna bağlı olarak immünoterapi tedavisine yanıtlarda baskılayıcı etki gösterir. Bu tez, invaziv olmayan MR/ MRS görüntüleme yöntemleriyle tümör pH'ının ölçülmesi ve immünoterapi yanıtlarının iyileştirmek için tümör asiditesini hedefleyen iki ana çalışmadan oluşmaktadır.

Bu tez kapsamında pH ölçümü için iki farklı MR görüntüleme tekniği geliştirdik. L-DOS47 tedavilerinden önce ve sonra pH'lardaki farklılığın kontrol farelerinden istatistiksel olarak anlamlı derecede yüksek olduğunu gösterdik. Bu, önerilen ilacın klinik öncesi modellerde nötrleştirme yetisini gösteren ilk çalışmadır.

Bu tezin ikinci amacı, klinikte hasta yararları için kullanılma potansiyeline sahip kombinasyon yaklaşımları geliştirmektir. Bu kapsamda, L-DOS47 tedavisi ile tümör asitliğinin nötralizasyonunun, anti-PD1 ile birleş tirildiğinde sağkalımı arttırmada etkili olduğunu fareler üzerinde gösterdik.

Genel olarak, bu tez çalışması kapsamında tümör pH'sinin ölçümü için MR ile iki görüntüleme tekniği geliştirdik. Ayrıca, immünoterapi yanıtlarını arttırmak için bir kombinasyon tedavisi modeli geliştirdik. Isovue, L-DOS47 ve anti-PD1'in, klinikte kullanılmak üzere FDA tarafından onaylanması bu çalışmayı yeni bir klinik deneme tasarımı için dikkate değer kılmaktadır.

**Anahtar Sözcükler:** Tümörlerin mikroçevresi, Kanser, İmmünoterapi, MR Görüntüleme.



## TABLE OF CONTENTS

ACKNOWLEDGMENTS . . . . .	iv
ACADEMIC ETHICS AND INTEGRITY STATEMENT . . . . .	vi
ABSTRACT . . . . .	vii
ÖZET . . . . .	viii
LIST OF FIGURES . . . . .	xi
LIST OF SYMBOLS . . . . .	xv
LIST OF ABBREVIATIONS . . . . .	xvi
1. MOTIVATION AND OBJECTIVES . . . . .	1
1.1 Thesis hypotheses and objectives . . . . .	2
2. THE EFFECT OF TUMOR MICROENVIRONMENT ON IMMUNE CELLS	1
2.1 Effect of hypoxia on immune function . . . . .	4
2.1.1 Effect of hypoxia on lymphocytes . . . . .	4
2.1.2 Effect of hypoxia on myeloid cells . . . . .	6
2.1.3 Effect of hypoxia on neutrophils . . . . .	7
2.1.4 Effect of hypoxia on dendritic cells . . . . .	7
2.2 Effect of acidosis on immune function . . . . .	8
2.2.1 Effect of acidosis on lymphocytes . . . . .	9
2.2.2 Effect of acidosis on myeloid cells . . . . .	10
2.2.3 Effect of acidosis on neutrophils . . . . .	10
2.2.4 Effect of acidosis on dendritic cells . . . . .	11
2.3 Targeting hypoxia and acidosis to improve immunotherapy . . . . .	11
2.3.1 Targeting hypoxia in combination with immunotherapy . . . . .	12
2.3.2 Targeting acidosis in combination with immunotherapy . . . . .	13
3. MAGNETIC RESONANCE IMAGING OF TUMOR MICROENVIRONMENT	15
3.1 Hyperpolarized Magnetic Resonance Imaging . . . . .	16
3.1.1 <sup>15</sup> N and <sup>13</sup> C Hyperpolarized Magnetic Resonance Spectroscopy to determine the action of urease enzyme . . . . .	17
3.2 Phosphorus-31 Magnetic Resonance Spectroscopic Imaging . . . . .	18
3.2.1 <sup>31</sup> P MRSI of tumor microenvironment . . . . .	19

3.3	Chemical Exchange Saturation Transfer (CEST) MRI . . . . .	22
3.3.1	CEST of tumor microenvironment . . . . .	23
4.	TARGETING TUMOR MICROENVIRONMENT TO IMPROVE IMMUNOTHER- APY RESPONSES . . . . .	30
4.1	Introduction . . . . .	30
4.1.1	Microenvironment modifier drug: L-DOS47 . . . . .	31
4.1.2	Immunotherapy . . . . .	32
4.2	Generation of Cancer Model to be Used for the Study . . . . .	33
4.2.1	LKR/CEACAM6 preclinical model . . . . .	33
4.2.2	Panc02/CEACAM6 preclinical model . . . . .	37
5.	OVERALL CONCLUSIONS . . . . .	46
	APPENDIX A. LIST OF PUBLICATIONS PRODUCED FROM THE THE- SIS . . . . .	50
	REFERENCES . . . . .	51

## LIST OF FIGURES

Figure 2.1	Illustration of the cellular components of tumour microenvironment.	2
Figure 2.2	Tumor physical microenvironment (hypoxia and low pH) can modulate immune cells to enhance tumor growth.	3
Figure 3.1	A 10 cc syringe containing 1 mL of urease solution was placed in an animal bed and 3 cc of hyperpolarized sample was injected into the magnet with a connection line from out of the magnet, in order not to move the bed during scan.	18
Figure 3.2	(a) Conversion of HP $^{15}\text{N}$ Urea to $\text{NH}_3/\text{NH}_4^+$ . $^{15}\text{N}/^1\text{H}$ 30 mm Doty coil was used to acquire spectrum. (b) Conversion of HP $^{13}\text{C}$ Urea to $\text{CO}_2/\text{HCO}_3^-$ . $^{13}\text{C}/^1\text{H}$ 30 mm Doty coil was used to acquire spectrum. As expected, $\text{CO}_2$ produced first and followed by $\text{HCO}_3^-$ . Besides the ratio of $\text{HCO}_3^-/\text{CO}_2$ gives the measure of pH.	18
Figure 3.3	(a) Spectra acquired from 3-APP phantoms. $\alpha$ -NTP was used as a reference for 3-APP spectra and calibrated to have the peak at -10.05 ppm. (b) Calibration curve for 3-APP. Dots represent chemical shifts obtained from phantom spectra.	20
Figure 3.4	Flow cytometry analysis for verification of CEACAM6 expression by BxPC3 cells.	21
Figure 3.5	$^{31}\text{P}$ MRS of 3-APP for saline and L-DOS47 injected mice before and 24 hours after each treatment. As clearly seen from the figures 3-APP chemical shifts, which are pH dependent, fit into together for control mouse while the L-DOS47 injected one shows shifting to the right.	22

Figure 3.6	The differences in tumor pHs for each mouse were determined before and 24 hours after saline/L-DOS47 treatments. The starting average pHs were $6.8 \pm 0.15$ and $6.7 \pm 0.19$ for saline and L-DOS47 treatment groups, respectively. Increase in tumor pH was higher for L-DOS47 injected mice ( $p < 0.05$ ).	22
Figure 3.7	T2 anatomical image of the phantom.	24
Figure 3.8	Calibration curve for CEST of Iopamidol. Dots represent experimental data	25
Figure 3.9	Stability test with phantom for 8 different conditions. Signal intensity and standard deviations were calculated for each scan to determine the best parameters for in vivo imaging.	26
Figure 3.10	Flow cytometry analysis for verification of CEACAM6 expression by Panc02 cells.	27
Figure 3.11	CEST MRI of iopamidol for pH imaging of a Panc02 clone 38 SC tumor. (a) T2 weighted image, CEST MRI (b) before L-DOS47 injection, (c) 30 minutes after $90 \mu\text{g}/\text{kg}$ L-DOS47 injection. L-DOS47 was administered iv while iopamidol was injected next to the tumor. M2M 30 mm $^1\text{H}$ coil was used for the experiment.	28
Figure 3.12	CEST MRI of iopamidol for pH imaging of a Panc02 clone 38 orthotopic tumor. (a) T2 weighted image, CEST MRI (b) before L-DOS47 injection, (c) 30 minutes after $90 \mu\text{g}/\text{kg}$ L-DOS47 injection. L-DOS47 and iopamidol were administered iv. M2M 30 mm $^1\text{H}$ coil was used for the experiment.	29
Figure 4.1	Master mix preparation for RT-PCR.	34
Figure 4.2	Melting curves for RT-PCR experiment.	35
Figure 4.3	Gel image for PCR products.	35
Figure 4.4	LKR parental and Clone 13 Cells were stained with Urease/L-DOS47 as negative and positive controls respectively. CEACAM6 expression for LKR clone was verified to be 90% with flow cytometry.	36


Figure 4.5	Average and individual volumes for 129S4/SvJaeJ mice injected with LKR Clone 13 cells. 13 days after tumor inoculation, regression in tumor growth in all groups was observed. As seen from data for individual mice, there were mice with complete response in all groups.	37
Figure 4.6	Workflow for infection experiments in order to provide expression of CEACAM6 antigen.	38
Figure 4.7	CEACAM6 expression for Panc02 clones were verified with flow cytometry.	39
Figure 4.8	Comparison of tumor growth for Panc02 Parental and CEACAM6 expressing clone (Clone 38) injected mice. Regression was not observed in tumor growth for this model.	39
Figure 4.9	Flow cytometry analysis for Panc02 parental, CEACAM6 15 and 38 clones.	40
Figure 4.10	In-vivo titration of L-DOS47 for Panc02 Clone 15 and Clone 38 injected mice. Results have shown that Panc02 clone 15 and clone 38 responded similarly to L-DOS47 therapy.	41
Figure 4.11	Average and individual tumor volumes for mice in each group (Saline, L-DOS47, Anti-PD1 and combination.) Addition of L-DOS47 to anti-PD1 treatment boosted the effect of immunotherapy on tumor growth.	42
Figure 4.12	Average tumor volumes for entire experiment and at endpoint with respect to different doses of anti-PD1. 15 $\mu\text{g}/\text{kg}$ twice a week is the most effective followed by 15 $\mu\text{g}/\text{kg}$ once a week. Interestingly 1.7 $\mu\text{g}/\text{kg}$ group was more effective than 5 $\mu\text{g}/\text{kg}$ group.	43
Figure 4.13	Flow cytometry analysis for Panc02 Parental, Clone 38 and Clone15 cells to determine CEACAM6 expression.	43

Figure 4.14 Average tumor volumes for entire experiment and at endpoint for saline and anti-PD1 treated mice injected with either Clones 15/38 and parental Panc02 cells. Tumors were growing faster for Panc02 Clone 38 cells injected mice for both anti-PD1 and saline treated groups compared to Panc02 Parental and Clone15 cells. 44

Figure 4.15 Kaplan Meier curve generated for 4 in vivo L-DOS47 & anti-PD1 combination experiments. The p value was determined as 0.0001 for the difference in survival between combination and saline groups. This value was 0.0568 for the difference between combination and anti-PD1 groups. 45

## LIST OF SYMBOLS

T	Tesla
H	Hydrogen
C	Carbon
N	Nitrogen
K	Kelvin
P	Phosphorus
W	Watt



## LIST OF ABBREVIATIONS

MRI	Magnetic Resonance Imaging
MRSI	Magnetic Resonance Spectroscopic Imaging
NK Cells	Natural Killer Cells
DC	Dendritic Cells
CTLA-4	Cytotoxic T Lymphocyte Antigen-4
PD-1	Programmed Cell Death Protein-1
PD-L1	Programmed Death Ligand-1
TCR	T-Cell Receptor
Treg cells	Regulatory T cells
TGF- $\beta$	Transforming Growth Factor- $\beta$
IL-10	Interlukin-10
M1	Classically-Activated Macrophages
M2	Alternatively-Activated Macrophages
TAM	Tumor Associated Macrophages
MDSC	Myeloid-Derived Suppressor Cells
VEGF	Vascular Endothelial Growth Factor
HIF1 - $\alpha$	Hypoxia Inducible Factor- $\alpha$
cAMP	Cyclic Adenosine Monophosphate
IFN- $\gamma$	Interferon- $\gamma$
Th2	T helper type-2
MICA	MHC class I Chain-related molecule A
NK2D	Natural Group 2D
ARG1	Arginase 1
Tie2 <sup>+</sup>	Angiopoietin 2
PHD-2	Prolyl Hydroxylase Enzyme-2
PHD-3	Prolyl Hydroxylase Enzyme-3
NF- $\kappa$ B	Nuclear Factor- $\kappa$ B
iNOS	Inducible Isoform of Nitric Oxide Synthase



DNP	Dynamic Nuclear Polarization
SNR	Signal-to-Noise Ratio
RF	Radiofrequency
P <sub>i</sub>	Inorganic Phosphate
NTP	Nucleoside Triphosphates
PCr	Phosphocreatine
3-APP	3-aminopropylphosphonate
TE	Echo Time
TR	Repetition Time
Hz	Hertz
i.p.	Intraperitoneally
i.v.	Intravenously
CEST	Chemical Exchange Saturation Transfer
CT	Computed Tomography
FOV	Field of view
ST	Saturation Transfer
sc	Subcutaneously
CEACAM6	Carcinoembryonic antigen-related cell adhesion molecule 6
ADC	Antibody Drug Conjugates
ADEPT	Antibody Directed Enzyme Prodrug Therapy
CAR-T cells	Chimeric Antigen Receptor T cells
RT-PCR	Real Time Reverse Transcription Polymerase Chain Reaction
PFA	Paraformaldehyde

## 1. MOTIVATION AND OBJECTIVES

It is well-known that tumor microenvironment is heterogeneous as it consists of both cancer, stromal and immune cells as well as chemical signals and matrix proteins [1]. Tumor formation is supported by the interactions between those compartments. The acidity in tumor microenvironment is caused by inadequate blood perfusion, increased glucose production, inflammation and hypoxia [2], [3], [4]. Cancer cells ferment glucose independently of oxygen presence (the Warburg Effect), which is followed by the production of lactic acid in extreme amounts [5], [6]. Acid-base regulators and monocarboxylate transporters facilitate the export of protons and lactic acid from tumor cells into the extracellular matrix, leading to acidosis in the tumor microenvironment [6], [7], [8].

Whereas the pH of blood and tissue is 7.2 - 7.4 under normal physiological conditions, in tumor microenvironment a local pH range from 5.5 to 7.0 is commonly observed [2], [3], [4], [6]. There is strong evidence that acidosis is usually allied with being immunodeficient [9], relatedly T cells could be exceedingly susceptible to acidic pH [10], [11].

Therapeutic resistance is critical in cancer prognosis. The acidic microenvironment of tumors have a remarkable affect on the efficacy of therapy outcomes including immunotherapies. Combining approaches with targeting tumor acidosis may conduct improved clinical trial design and overcome treatment resistance [12].

The role of targeting tumor acidosis on treatment outcomes is not recognized widely. However, recent study demonstrated that acidification promotes stroma or endothelium to produce inflammatory cytokines [13], [14]. Due to inflammatory signal induced by acidic tumor microenvironment, T cells cannot initiate until the acidosis is reversed. In tumors, neutralizing pH with buffers may provide improvement the response by promoting T cell activation [14].

In the scope of this work, new concepts were developed that can alter paradigms regarding acidosis as an anti-cancer immune suppressor and its neutralization as a combination therapy to improve therapy response. In this context, two robust and reproducible protocols for tumor pH measurements were developed and optimized with Magnetic Resonance Imaging.

## 1.1 Thesis hypotheses and objectives

The focus of the project is to target acidic microenvironment of tumors to improve immunotherapy responses. Hypotheses and objectives were as following:

(i) Hypothesis 1 - Developing techniques to measure the pH of tumor microenvironment with Magnetic Resonance -Spectroscopic- Imaging (MRI & MRS): In order to determine the pH of tumor microenvironment, several Magnetic Resonance Imaging (MRI) methods have been developed. However; while tumor acidosis and its consequences are critical, there is not an accomplished clinical instrument present to image tumor pH [15]. In the scope of this PhD work in vivo pH measurements by using state-of-the art techniques were established. These developments will make important contributions for coming clinical trials where in pH can be used as a biomarker and/or inclusion criteria for patients.

(ii) Hypothesis 2 - Targeting tumor microenvironment to improve immunotherapy responses: Targeting metabolic pathways to neutralize tumor pH is crucial to boost immunotherapy responses. On the basis of previous work, as a combination of buffer therapy and immunotherapy is promising but there is still area needs to be filled to conduct it to clinic. Considering this situation, combinatorial therapy with with a molecule which has high potential to be translated to the clinic was tested in the scope of this work.

In order to prove and support the hypotheses, objectives were specified. These are breaking the resistance of suppressing effects of tumor microenvironment on im-

mune cells (accordingly immunotherapy) and developing tools to image tumor pH and its neutralization.

(i) Objective 1 - Composing a review article describes the effects of tumor microenvironment on immune cells and how modulation of that can improve patient outcomes with respect to immunotherapy [16]. (Chapter 2)

(ii) Objective 2 - Developing non-invasive methods with MRI & MRS to measure tumor pH. (Chapter 3)

(ii) Objective 3 - Combining neutralization of tumor acidity with immunotherapy to improve therapy responses. (Chapter 4)

In the last chapter, overall conclusions and clinical relevance of the projects are given.

## 2. THE EFFECT OF TUMOR MICROENVIRONMENT ON IMMUNE CELLS

Damgaci, Sultan, et al. "Hypoxia and acidosis: immune suppressors and therapeutic targets." *Immunology* 154.3 (2018): 354-362.

Due to imbalances between vascularity and cellular growth patterns, the tumor microenvironment harbors multiple metabolic stressors including acidosis, which have significant influence on remodeling both tumor and peritumoral tissues. This stressor is also immunosuppressive and can contribute to escape from immune surveillance. Understanding these effects and characterizing the pathways involved can identify new targets for therapy and may redefine our understanding of traditional anti-tumor therapies.

Tumors commonly exhibit large amounts of intratumoral heterogeneity at genomic, physiologic, and anatomic scales. Tumors not only contain cancer cells, but are also massively infiltrated by host stromal cells [17] angiogenic vascular cells, cancer-associated fibroblasts, and cells of the immune system (Figure 2.1).

The immune system has roles on both cancer surveillance and tumor promotion [18]. Tumor associated immune responses contribute to various hallmarks of cancer including: sustaining tumor proliferative ability; resisting cell death, angiogenesis, invasion; promoting metastasis; evading growth suppressors; and avoiding immune destruction [19]. In order to prevent hyper activation of the immune cells, multiple suppressive mechanisms are employed to inhibit CD4<sup>+</sup> and CD8<sup>+</sup> T cell activities [20]. This inhibition is accomplished by Tregs by secretion of inhibitory cytokines such as interleukin-10 and Transforming growth factor , or by cytolysis through the secretion of granzymes by natural killer cells (NK cells) and CD4<sup>+</sup> T cells, or by metabolic disruption of the effector T cells , and targeting T cell functions via dendritic cells (DC) through cytotoxic T lymphocyte antigen-4 (CTLA-4) and other mechanisms [21]. CTLA-4 and PD-1 are

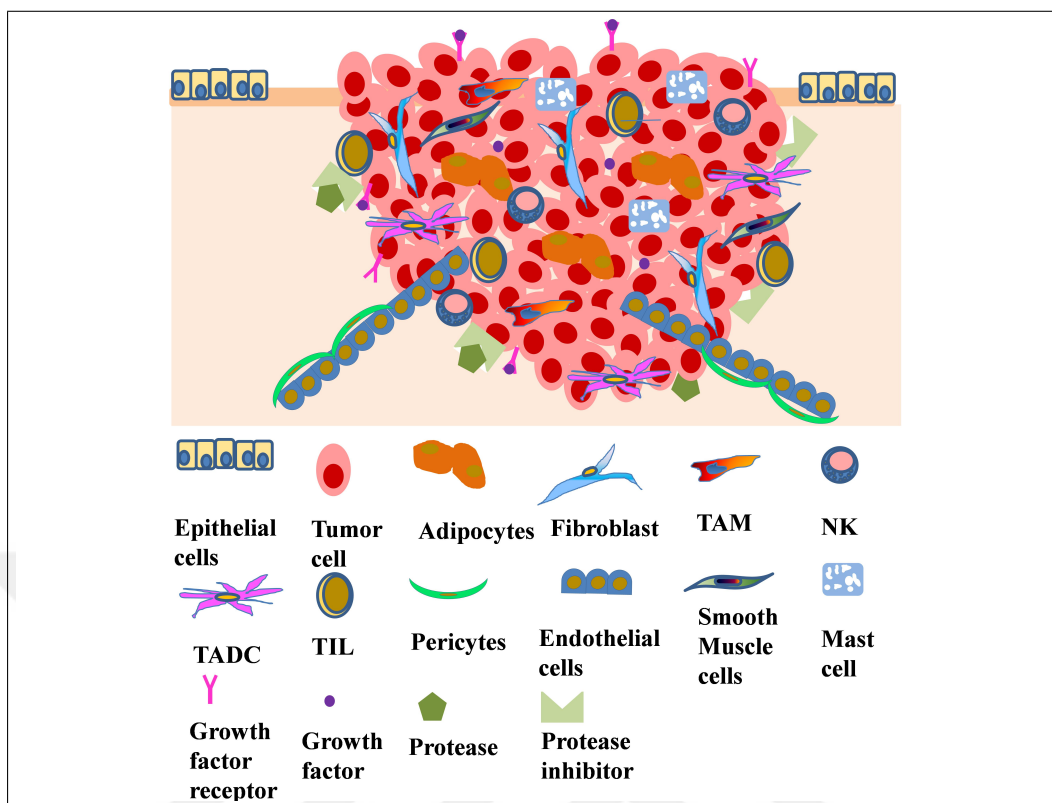


**Figure 2.1** Illustration of the cellular components of tumour microenvironment.

the two checkpoint receptors that have critical roles in cancer immunotherapy. CTLA-4 acts as a regulator for the early activation of naive and memory T cells. It is transported to the T cell surface and reduces TCR signaling. PD-1 restricts the activity of T cells in the periphery to control autoimmunity. It has two known ligands, PD-L1 (B7-H1) and PD-L2 (B7-DC). PD-L1, in particular, is upregulated in many cancers in response to proinflammatory cytokines and results in inhibiting local anti tumor T cell responses [22]. Macrophages alter their cell surface expression profile as they polarize between anti-inflammatory (M1) and pro-inflammatory (M2) phenotypes in response to external milieu and contribute to immunoregulation. "Classically-activated" M1 macrophages express CD80/CD86 molecules and can activate T cells. Additionally, M1 macrophages can display cytotoxic activity against pathogenic bacteria or neoplastic cells. "Alternatively-activated" M2 macrophages express immunosuppressive ligands [20]. During tumor progression, neoplastic cells evade immune surveillance by evolving mechanisms that subvert the normal tumor-specific immune response, such as distorting the macrophage populations to favor the M2 phenotype [23]. or over-

expression of checkpoint ligands [22]. Upregulated expression of immunosuppressive ligands, such as B7H4, on both tumor associated macrophages (TAMs) and tumor cells are also found in the tumormicroenvironment [24]. Myeloid-derived suppressor cells (MDSCs) are another type of immune suppressors in tumor microenvironment have known negative effects on T cell and NK cell functions [25]. This inhibition of immune surveillance via alternative activation of immune cells is mediated by ligand expression and cytokines, as well as soluble and physico-chemical factors of the tumor microenvironment [23] (Figure 2.2).

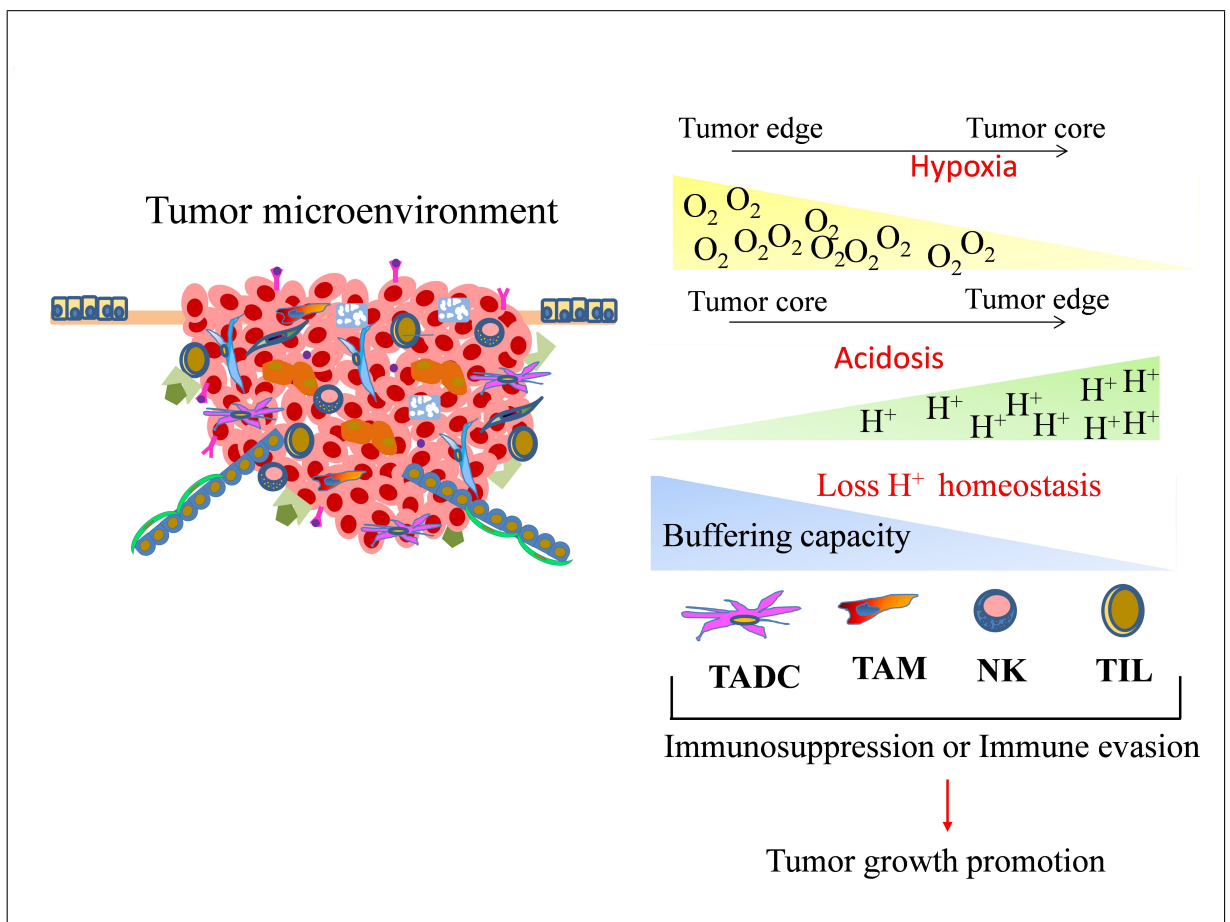


**Figure 2.2** Tumor physical microenvironment (hypoxia and low pH) can modulate immune cells to enhance tumor grow.

## 2.1 Effect of hypoxia on immune function

Hypoxia can be simply identified as lack of oxygen, which is a consequence of increasing oxygen requirement by proliferating cancer cells and dysfunctional and insufficient blood supply resulting from tumour angiogenesis [12]. As normal oxygen pressure varies between different tissues, there is not a fixed level to define hypoxia or degree of hypoxia. For instance, normoxia is a partial pressure of 21% in the lungs, 13% in arterial blood and 5% in the human liver [26], [27]. However, when the vessels are not developed and/or are blocked, e.g. in an ischaemic episode, the oxygen partial pressure decreases, leading to oxygen deficits with  $pO_2 < 1.5\%$  (c.10 mmHg), known as hypoxia. Although many tumours promote vessel formation through signalling via the vascular endothelial growth factor (VEGF), unregulated VEGF can actually lead to hyperproliferation of blood vessels, which leads to reduced perfusion due to imbalanced capillary networks [28], [29]. As described below, hypoxia has dramatic effects on all cells involved in immune reactivity.

### 2.1.1 Effect of hypoxia on lymphocytes

The three major types of lymphocytes are T cells, B cells and NK cells. T cells and B cells are major cellular components of the adaptive immune response to neoantigens, whereas NK cells are considered part of innate immunity. The effect of the hypoxia inducible factor ( HIF1 -  $\alpha$  ) pathway on T lymphocytes was reviewed by Palazon et al [30]. In vitro experiments have demonstrated that the concentration of oxygen in the culture media can modify the proliferation and function of T lymphocytes. Low oxygen levels significantly reduce lymphocyte proliferation, compared with normoxic conditions [31], [32]. This may have a physiological role, as lymph nodes and spleen contain large regions of hypoxia in vivo [33], and this is thought to prevent CD8<sup>+</sup> T-cell activation by stabilization of HIF1 -  $\alpha$  and suppression of TCR - mediated Ca<sup>2+</sup> signalling [34].

Hypoxia increases the FOXP3 transcription factor levels, which is a potent reg-



ulator of Treg cells [35]. Hypoxia also promotes the production of TGF- $\beta$  and CCL28, both of which have a role in the up-regulation of Treg cells, contributing to the inhibition of Teff cell responses, and also promoting angiogenesis and tumour tolerance [36], [37]. Further, hypoxia appears to skew CD4<sup>+</sup> cells towards a T helper type 2 (Th2) phenotype [38], and the resultant IL-4 can induce alternative macrophage polarization. HIF1- $\alpha$  regulates the balance between Treg cells and Th17 differentiation [39]. Additionally, it has been shown that the accumulation of extracellular adenosine linked to increased elevation of cyclic adenosine monophosphate (cAMP), promoted by the cAMP adenosine receptor A2AR, causes inhibition of antitumour activity of T cells [40]. Hypoxia negatively affects the production of interferon- $\gamma$  (IFN- $\gamma$ ) and IL-2 by both CD4<sup>+</sup> and CD8<sup>+</sup> T cells [41]. It was also observed that the performance and presence of T cells are decreased in hypoxic regions in vivo [42]. Hypoxia generates reactive nitrogen species by MDSC and TAMs. Nitration of TCR and CD8 cells decreases their ability for recognizing cognate MHC antigen. Besides, nitration of the chemokine CCL2 inactivates its capacity to attract effector lymphocytes while it can still attract MDSCs. HIF1- $\alpha$  prompts PD-L1 expression on tumour cells and MDSCs, which results in the suppression of Teff cells [43].

In NK cells, the relation between HIF1- $\alpha$  up-regulation of metalloproteinase ADAM10 and down-regulation of MHC class I chain-related molecule A (MICA), has an effect on resistance to lysis. Accordingly the interaction between natural group 2D (NK2D) and MICA plays a critical role in the direction of NK cell responses against tumour cells [44]. Up-regulation of TGF- $\beta$  by hypoxia can also decrease NKG2D receptors on NK cells, which may be due to hypoxia-induced release of microvesicles [45], [46], [47]. Further, hypoxia-induced autophagy leads to granzyme B degradation and allows tumour cells to escape from NK-mediated killing [48], [49]. The effects of hypoxia on reduced NK activity can also be indirect. For example, in melanoma cells, hypoxic stress increases the gap junctional Connexin43 expression in a HIF1- $\alpha$  dependent manner [50] and Connexin43 renders cells less susceptible to NK-cell-mediated lysis [51]. The cytotoxicity of NK cells in metastatic niches has been shown to be decreased by hypoxia, which was demonstrated by injecting mice with cells derived from hypoxic mammary tumour cells, resulting in increased MDSC infiltration and NK

inhibition [52].

### 2.1.2 Effect of hypoxia on myeloid cells

Macrophages are one of the most abundant types of myeloid cells in the tumour microenvironment. Their main function is to engulf and digest debris and foreign substances, including microbes, extracellular matrix remnants and tumour cells [53]. However, attracted by the hypoxic environment of tumour [54], TAMs can promote malignant progression in part by inducing angiogenesis [55], and matrix remodelling that supports progressively growing neoplasms [56]. Hypoxia promotes the expression of VEGF, fibroblast growth factor, and matrix metalloproteinases 7 and 9 genes by macrophages, which leads to an increase of macrophage infiltration into hypoxic regions, where they reduce inflammation to promote tumour progression [57]. It has been demonstrated in vivo that HIF1- $\alpha$  is required in the regulation of myeloid cell glycolytic capacity, survival and function in the inflammatory microenvironment [58].

Both TAMs and MDSCs often express Semaphorin 3A via Neuropilin binding, which helps both types of cells to enter hypoxic zones. As they enter, HIF1- $\alpha$  down-regulates Semaphorin 3A, resulting in the accumulation of these cells in hypoxic zones [45]. Studies in adenocarcinoma models support the idea that the M1 phenotype of TAMs dominates in the normoxic niches, whereas the M2 phenotype of TAMs dominates in hypoxic niches [59]. Different types of HIF activity of TAMs have also been observed. HIF1- $\alpha$  is stabilized during M1 polarization, which involves nuclear factor - $\kappa$ B [60], [61], [62], [63], whereas HIF2- $\alpha$  is stabilized during M2 polarization [64], [65]. The consequences of this differential expression of HIFs are not known, although it has been shown that HIF2- $\alpha$  is an important regulator of arginase1 gene expression, a molecular marker of M2 polarization [66]. During oxygen deficiency, HIF1- $\alpha$  is stabilized in TAMs, which is associated with the increase of transcription and secretion in VEGF, crucial for pro-tumoral angiogenesis. TAMs that express angiopoietin 2 (Tie2<sup>+</sup>), induced by hypoxia in monocytes, are profoundly pro-angiogenic [67]. HIF1- $\alpha$  expression by TAMs is also known to be responsible for the suppression of T-cell

responses [68] and promotes PD-L1 expression on MDSCs [43].

### 2.1.3 Effect of hypoxia on neutrophils

Neutrophils are phagocytic granulocytes that are mediators of innate immunity. Despite their short lifespans, they are the most abundant class of white blood cells in humans. There is a link between the high rate of tumour invasiveness and elevated neutrophils and those neutrophils are stabilized by hypoxia [69]. Hypoxia promotes neutrophil survival in a HIF1- $\alpha$  mediated manner [63], which promotes a loss of host defence function of neutrophils. Degradation of HIF1- $\alpha$  is promoted by activation of prolyl hydroxylase enzymes, PHD-2 and PHD-3. A direct and specific role for PHD-3 in promoting neutrophil survival in hypoxia has been observed using PHD3-deficient neutrophils [70]. It is possible that the effect of hypoxia on neutrophil longevity is mediated by a significant inhibition of neutrophil apoptosis, which is the major mechanism involved in the resolution of inflammation. This effect of hypoxia on neutrophil apoptosis has been shown in vitro to be a bcl-2-independent process [71]. The mechanisms by which hypoxia regulates neutrophil survival have been studied, and it was shown that induced survival is mediated by HIF1- $\alpha$ dependent activity [63]. Hypoxia also appears to impair neutrophil chemotactic migration in vitro [72].

### 2.1.4 Effect of hypoxia on dendritic cells

Dendritic cells are antigen-presenting cells that play an important role in connecting innate and adaptive immunity. There are few studies investigating the effect of hypoxia on DCs. In contrast to other immune system cells, hypoxia appears to improve the activity of DCs, which may have a physiological role, as lymph nodes are known to be hypoxic [33]. Hypoxia and HIF1- $\alpha$  regulate DC maturation, activation and antigen-presenting functions [73]. Hypoxia regulates expression of co-stimulatory molecules CD80 and CD86 by DCs. Dendritic cells stabilized HIF1- $\alpha$  and this resulted in a stronger T-cell activation and proliferation with PHD inhibition. HIF1- $\alpha$  also

hinders differentiation of bone marrow precursors into plasmacytoid DCs [46].

## 2.2 Effect of acidosis on immune function

In contrast with hypoxia, studies on the effect of low pH on the immune system are less well developed, despite its near-universal presence in solid tumors. Tumor acidosis is a phenomenon of tumor progression, and results from elevated fermentative carbohydrate metabolism combined with poor perfusion. During carcinogenesis, cancer cells are selected by stressful conditions to ferment glucose, even in the presence of adequate oxygen [4]. Even though aerobic glycolysis (fermentation) is less efficient than respiration for energy production, it is one of the most commonly observed phenotypes in cancers. A significant consequence of increased glycolysis is acidification of the extracellular milieu and some have proposed that cancer cells that produce acid are more competitive and hence, acidity itself, rather than glycolytic ATP production or access to anabolic substrates, is the selected phenotype [74].

Releasing lactate at high rates is also a strategy to overcome immune surveillance. Some studies investigate lactate without changing pH, and others focus on acidosis without changing lactate [14], whereas both are changing simultaneously in vivo. Those studies that have investigated both in concert have observed that low pH exacerbates lactate effects and vice-versa. Lactate is a promoter of tumor acidity, local invasion and matrix remodeling [75]. This acidity has direct effects on the immune system.

The acidic tumor microenvironment has multiple consequences relevant to carcinogenesis, including somatic selection of cancer cells during initial phase of tumorigenesis for augmented cell survival, escape from apoptosis, and drug resistance [76]. More recent studies also demonstrated that acidosis can alter the functions of cells of the immune system, including T cells, neutrophils, macrophages and DCs [23], [77].

### 2.2.1 Effect of acidosis on lymphocytes

Both cancer and immune cells are highly dependent on the glycolytic pathway for proliferation, survival, and activity. Cancer cells rely on glycolysis even under aerobic conditions and may be due to rapid temporal changes in energy demands for cell membrane activities needed for division, growth and migration [78]. This allows cancer cells to rapidly adapt to changing conditions more effectively than non-glycolytic cells. Furthermore, elevated glycolysis significantly reduces glucose availability and, while cancer cells can enter in quiescence in the absence of glucose, activated T cells do not survive without glucose. Thus, reduced glucose alone puts T cells at a disadvantage when attempting to expand into an acidic environment [79].

An acidic tumor microenvironment does not appear to affect CD4+ Tregs, possibly because they primarily rely on fatty acid oxidation [80]. In contrast to CD4+ cells, acidification profoundly induces an anergic state in both human and mouse tumor-specific CD8+ T lymphocytes. This results in severe reductions in cytolytic activity, cytokine secretion, downregulation of IL-2Ra (CD25) and TCR followed by diminished activation of STAT5/ERK signaling [81]. It is also reported that low pH affects plasma membrane and microtubule mobility, leading to decreased association of different TCR components with CD8 or other co-receptors, thus contributing to T cell anergy [82]. It has been shown in vitro that raising the culture pH can reverse T cell anergy and that long-term exposure to low pH can cause permanent damage or induce T cell apoptosis. In the short term, however, acidosis leads to increased persistence, presumably because of the aforementioned anergy.

Lymphocyte motility under low pH microenvironments has also been investigated. Stimulation of murine splenic lymphocytes with IL-2 in three-dimensional gels showed that acidic pH increases the migration of lymphocytes through the extracellular matrix. Excitation and performance of T-cells are blocked by acidity in vitro by separation of interferon-gamma mRNA and that this is related with metabolic changes that are not mediated by acidification of cytoplasmic pH. It was demonstrated with this study that neutralization of tumor pH with oral buffer was resulted with enhanced out-

comes for checkpoint inhibitors and adoptive T cell transfer [14]. Furthermore, tumor acidity promotes tumor progression by negatively affecting maturation and function of TH1 lymphocytes while stimulating the progression of tumor-promoting TH2 lymphocytes by inactivation of IFN- $\gamma$  and suppression of TNF- $\alpha$  [79].

### 2.2.2 Effect of acidosis on myeloid cells

The influence of pH on macrophage polarization is less well documented. Some studies focused on the effect on tumor angiogenesis, and showed that the process of activation and transformation of the TAMs into a pro-angiogenic phenotype in breast cancer is stimulated by low pH and high lactate concentrations [83].

Lactate has been found to be responsible for promoting survival and proliferation of MDSC [84] 30 and increase the release of pro-angiogenic factors by the murine macrophage cell line RAW264.7 via induction of VEGF production and release. In contrast, another study has shown that there is no effect of low pH on angiogenic activity of human macrophages. Other studies of low pH effect on regulation of macrophages have been focused on activation of inducible isoform of nitric oxide synthase (iNOS). Macrophages exposed to low pH had an elevated iNOS level in a NF- $\kappa$ B dependent manner, which can be activated by TNF- $\alpha$  [85]. Lactic acid produced by tumor cells affects signaling through the induction of VEGF and M2 like polarization of TAMs [86], and gives rise to the expression of arginase 1 (ARG1) in macrophages to inhibit T-cell proliferation and activation. Consistent with this, we have observed that adaptation of macrophages to low pH induces an M1  $\rightarrow$  M2 phenotypic switch, characterized by a loss of iNOS and induction of arginase and the mannose receptor, CD206 [87]. .

### 2.2.3 Effect of acidosis on neutrophils

The effect of acidosis on neutrophils was comprehensively reviewed in 2001 by Lardner in which it was pointed that acidic pH leads to decrease of superoxide pro-

duction [10]. Acidosis can also elicit human neutrophil activation through transient up-regulation of CD18 expression, increase in  $\text{Ca}^{+2}$  over resting levels, and delays in rate of apoptosis [88]. Acidosis-induced neutrophil activation occurs via phosphatidylinositol 3-kinase/Akt and ERK pathways [89].

#### **2.2.4 Effect of acidosis on dendritic cells**

Studies investigating the effect of acidosis on DC behavior found that extracellular acidity improved the antigen-presenting capacity of DCs derived from murine bone marrow [90]. In this study, lactic acid either alone or with combination of the tumor-derived cytokines macrophage colony-stimulating factor and IL-6, significantly altered antigen presentation and functional activity of DCs, pointing to a possible metabolic effector function of lactate independent of its effects on pH.

### **2.3 Targeting hypoxia and acidosis to improve immunotherapy**

Immunotherapy is a growing and promising field that can lead to improved control of cancers with high mutational loads (neo-antigens). The prominent types of immunotherapy include immune checkpoint inhibitors, cancer vaccines, and adoptive T cell transfer. Although significant progress has been made, durable response rates remain low. For instance, objective response rates in melanoma are from 18% to 27% for anti-PD-1 or PD-L1 antibodies, and 11% for anti-CTLA-4 antibodies. Notably, the combination of PD-1 and CTLA-4 checkpoint blockades showed an increase in response when compared with using either checkpoint alone, from 20% to 40%. This implies, however, that 60% of patients are nonresponsive and thus, other immunosuppressive activities are likely present. An underexplored inhibitor of immunotherapy is the impact of physical tumor microenvironment on immune function. Given the above evidence of the impact acidosis on immune function, it is reasonable to expect that manipulating the microenvironment will enhance outcomes of immunotherapy in some patients, especially if they are biomarker driven.

### 2.3.1 Targeting hypoxia in combination with immunotherapy

Hypoxia influences immune checkpoint receptors and their respective ligands. HIF1- $\alpha$  and HIF2- $\alpha$  were both investigated in relation to PD-L1, whose promoter contains a hypoxia-response element. Importantly, hypoxia selectively up-regulates PD-L1 on MDSCs through HIF1- $\alpha$ . This was not limited to MDSCs, as hypoxia also significantly increased PD-L1 expression on macrophages, DCs and tumour cells [43]. Combinatorial approaches using HIF1- $\alpha$  inhibitors with PD-L1 blockade may boost immune responses in patients [91]. Another combinatorial approach using a HIF1- $\alpha$  inhibitor with DC-based immunotherapy resulted in tumour regression and improved survival in a mouse model of breast cancer [92].

Alternatively, targeting tumour hypoxia directly may enhance immunotherapy responses by decreasing the number and function of immunosuppressive cells, increasing effector T cells and improving vaccine efficacy. Tumour cells adapt to hypoxia by angiogenic switch with production of VEGFs, angiopoietin-2, IL-8 and other factors. As dysfunctional vessels lead to hypoxia and tumour resistance there is a strong effect to normalize vessels to reduce hypoxic volumes within the tumour microenvironment. Normalizing vessels by targeting VEGF/VEGFR promotes CTL entry to tumour mass. It also affects macrophage polarization and stimulates M1 phenotype. Inducing Th1 and triggering secretion of IFN- $\gamma$  and IL-12 allows CTL infiltration which triggers decrease in Treg cells [93]. Targeting hypoxic regions with hypoxia-activated pro-drugs, evofosfamide (TH-302), improved checkpoint blockade (CTLA-4, PD-1) in transplantable and genetically engineered prostate cancers in preclinical models [94]. Hypoxia-specific cytotoxic activity of hypoxia-activated pro-drugs was observed with in vivo and in vitro models [95], [96]. Based on these and other data, a clinical trial (NCT03098160) combining evofosfamide with ipilimumab in solid tumours was opened in May 2017.



### 2.3.2 Targeting acidosis in combination with immunotherapy

Therapies based on manipulating of tumor micro-environmental acidosis using buffers have shown improved results as monotherapy in a variety of animal cancer models [97], [98], [99], [100]. According to preliminary studies, neutralizing tumor acidosis with buffers in combination with immunotherapy can lead to improved durable outcomes [14]. In this study, oral bicarbonate buffer (200 mM ad lib) was used to neutralize tumor acidity and, in combination with anti-CTLA-4, anti PD-1, or adoptive T cell therapy, led to durable responses in both B16 melanoma and Panc02 pancreatic cancer models. These findings suggest that buffer therapy may improve response rates to immune therapies in the clinic. However, a buffer therapy approach is not easy to implement clinically as three clinical trials (NCT-1350583, NCT-01198821, and NCT-1846429) were not successful due to poor patient compliance and grade 2 GI events. Another approach to increase tumor pH directly is utilizing the action of urease enzyme. Ureases are urea degrading enzymes which convert urea into more toxic ammonia and lead to local pH rise from the generated ammonia [101]. CEACAM6-targeted Jack bean urease (L-DOS47) has begun to be used in preclinical tumor models and clinical trials to modify tumor microenvironment [102].

There are numerous possibilities to target tumor acidity more indirectly by influencing metabolism or ion transport. For example, Carbonic Anhydrase IX (CA-IX) controls intra- and extracellular acid-base balance to maintain survival and is a key regulator of extracellular acidity. As a catalyzer of reversible hydration of  $\text{CO}_2$  to bicarbonate and protons at the extracellular surface, inhibition of catalytic activity of CA-IX can manipulate its role in pH regulation [12]. Lactate overproduction is another hallmark of cancer which is associated with acidity and can impact a cells ability to regulate its pH in the face of acidity [103]. As tumor cell's need slightly alkaline intracellular pH, they overcome the accumulation of lactate and  $\text{H}^+$  ions in terms of using monocarboxylate transporters (primarily MCT-4) that facilitate the export of lactate and  $\text{H}^+$ . By reversing the molecular machinery, cancer cells provide alkaline intracellular media while having external acidic pH, which is also beneficial for survival and invasive characteristic of cancer cells. Furthermore, there is a mutual metabolic

relationship between cancer and stromal cells. In contrast to the belief that stromal cells use only glucose as an energy source, it was demonstrated that they also can use cancer cell-derived lactate, which is transported into cells primarily with MCT-1 [104]. There is a strong effort to target MCTs, and these approaches may be combined with immune therapies by virtue of their effects on pH regulation [12]. Targeting lactate metabolism is another promising approach for modulation of tumor pH. High glycolysis rates in cancer cells result with lactate overproduction. As cancer cells export lactate rather than using as a nutrient, it acidifies the tumor microenvironment [105]. One such approach could be targeting Lactate dehydrogenase A, LDHA, which has been shown to inhibit pyruvate to lactate in vivo conversion [106], [107]. On the other hand, usage of LDHA inhibitors is challenging as it was reported that LDHA deletion in CD4 T cells show defects in IFN- $\gamma$  production [108].

Until recently, the primary approach to treating cancer has been the identification of genetic instabilities with gene product targeted therapies, which has failed to lead to durable responses. The emergence of immune targeted therapies has led to more durable responses, although response rates remain low. More recently, the role of tumor microenvironment's effect on the immune system has begun to be studied. Both hypoxia and tumor pH have direct and indirect effects on immune system and are, in general, "immune suppressors". There is strong evidence that hypoxia and low pH can contribute to resistance to immune therapies. Although important progress has been made to understand the mechanisms underlying the effects of hypoxia and low pH on immunotherapy, non-negligible knowledge gaps still remain. There is strong evidence that hypoxia and acidic pH in the tumor microenvironment have dramatic effects on immune system cells and therapeutic resistance. New treatments that aim to perturb them is an intriguing avenue for further improving responses to immunotherapy.

### 3. MAGNETIC RESONANCE IMAGING OF TUMOR MICROENVIRONMENT

Solid tumors are unequivocally acidic [109], [110]. The concept that tumor acidosis inhibits immune surveillance has been increasingly appreciated over the past 5-6 years [81], [10], [16]. Indeed, neutralization of acidity dramatically improves response to checkpoint blockade and adoptive cell transfers [14]. Despite this promise, phase I/II clinical trials of bicarbonate (NCT-1350583 and NCT-01198821) failed to accrue because of patient incompliance and gastrointestinal issues [111]. Hence alternative approaches are needed to neutralize tumor acidity. CEACAM6-targeted urease, L-DOS47 (Helix Biopharma), can target tumor microenvironment directly to provide local pH increase. L-DOS47 is already in a phase I/II trial (NCT-02309892), well-tolerated and dose escalated. CEACAM6 is over-expressed in lung and GI cancers including pancreatic [112]. Urease converts endogenous non-ionized urea into 1X CO<sub>2</sub> and 2X NH<sub>3</sub>, which rapidly ionize to HCO<sup>3-</sup> and NH<sub>4</sub><sup>+</sup>, thus consuming a net H<sup>+</sup> in the process and directly raising the local pH.

Imaging pH as an inclusion criteria and to guide for treatment decisions-changing directions are critical for personalized medicine. Tumor pH can be a good biomarker candidate to be translated to clinic for patient benefits. Several clinical and pre-clinical studies have shown promise that clinical acidosis monitoring will be available in the near future.

In this chapter, the urease enzyme activity with Hyperpolarized MRI was demonstrated for the first time. Besides, in order to identify the tumor microenvironment two -non invasive- methods were developed for tumor pH measurements with MRI. The effect of L-DOS47 on tumor pH was determined using those techniques.

### 3.1 Hyperpolarized Magnetic Resonance Imaging

Hyperpolarized Magnetic Resonance Imaging (MRI) can be employed to determine the real-time tumor metabolism. Dissolution dynamic nuclear polarization (DNP) method increases sensitivity of labelled molecules such as  $^{15}\text{N}$  and  $^{13}\text{C}$  which can be injected to the animal during scanning.

Hyperpolarized Magnetic Resonance Imaging (MRI) can be employed to determine the real-time tumor metabolism. Dissolution dynamic nuclear polarization (DNP) method increases sensitivity of labelled molecules such as  $^{15}\text{N}$  and  $^{13}\text{C}$  which can be injected to the animal during scanning. [113]. The solutions and metabolite concentration are adjusted to have glass composition in low temperature, which facilitates the polarization assignment from free radical to nearby labeled nuclei [114]. The magnetic fields of commercial polarizers are  $\sim 3$  Tesla while temperatures are maintained near 1K. Under these conditions, electrons are  $\sim 100\%$  polarized whereas nuclei are only polarized in  $\sim 0.1\%$ . Microwaves transfer electron polarization to the nuclei, which can thus be polarized to 10 - 30 % or an increase of approx. 10,000-30,000 fold. In order to eject the polarized sample from the polarizer, a quick dissolution process is performed which is done by pumping a preheated buffer through the polarizer to melt the hyperpolarized substrate and discharge it from the machine. The polarization process can take up to 2 hours and provides  $10^5$  - fold increase in spin polarization which allows high signal-to-noise ratio (SNR) spectra to be acquired in less than a second. Polarization generally lasts  $< 2$  minutes and each radiofrequency (RF) -acquisition- destroys of hyperpolarization since spin returns to their equilibrium state through  $T_1$  relaxation [115]. Since the time is limited after taking out the sample from polarizer, experiments should be designed to acquire high SNR data with minimal loss of polarization. Small flip angles are commonly used to minimize the RF-based losses. Fast imaging sequences in which each metabolic map recorded after each RF pulse are preferred mostly because of the reasons listed. There is no need to wait for signal to recover after RF pulses which allows to use shorter repetition times, which is especially useful when more than RF pulse is required in the same imaging session [116].

### 3.1.1 $^{15}\text{N}$ and $^{13}\text{C}$ Hyperpolarized Magnetic Resonance Spectroscopy to determine the action of urease enzyme

L-DOS47 targets/binds to the human CEACAM6 antigens and the urease part of the drug converts urea to ammonia. This conversion is resulted with the increase of pH in tumor microenvironment. In order to observe the action of urease and the products of the reaction Hyperpolarized Magnetic Resonance Spectroscopy (HP-MRS) technique was used.

Hyperpolarized urea samples were prepared with 3.1 g of either  $^{13}\text{C}$  or  $^{15}\text{N}$  Urea, 7.15 g glycerol, 0.216 g OX63 (free radical) and 0.75 mM Gadavist with a combination of vortex mixing and bath sonication with heat (60 °C), followed by glassing at low temperature. Samples were hyperpolarized in an Oxford Hypersense Dynamic Nuclear Polarizer by irradiation with 93.38 GHz microwaves in a field of 3.35 T at approximately 1.2 K. Hyperpolarized samples were dissolved in  $\sim 3$  mL sodium hydroxide solution (3.2 gr of sodium hydroxide, 100 mg Disodium EDTA hydrate, 5.6 g Trizma preset crystals pH=7.4, 2.9 g sodium chloride and 1L DI water).

In order to demonstrate urease activity, phantoms were first prepared using a syringe system of our design wherein hyperpolarized substrates can be injected directly into the magnet (Figure 3.1). In these studies, a 10 cc syringe containing 4 ml of 10 mM urea solution was placed in the magnet and shimmed. When conditions were optimized to get an SNR of 35 this solution was replaced with 1 mL urease solution (150-500 units/ml) and spectra were acquired every 3 sec for 5 minutes following bolus injection of 3 cc hyperpolarized  $^{13}\text{C}$  or  $^{15}\text{N}$  urea to measure the time-dependent conversion of urea to  $\text{CO}_2/\text{HCO}_3^-$  and  $\text{NH}_3/\text{NH}_4^+$  (Figure 3.2). Acquisition conditions were as following. TR: 3000 ms, Flip Angle:  $5^\circ$ , Acquisition points: 1028, Acquisition Bandwidth: 10 KHz, Dwell time: 50  $\mu\text{s}$ , Spectral resolution: 4.86 Hz/points.  $^{15}\text{N}/^1\text{H}$  and  $^{13}\text{C}/^1\text{H}$  30 mm Doty coils were used to acquire spectra from  $^{15}\text{N}$  and  $^{13}\text{C}$  Urea samples.

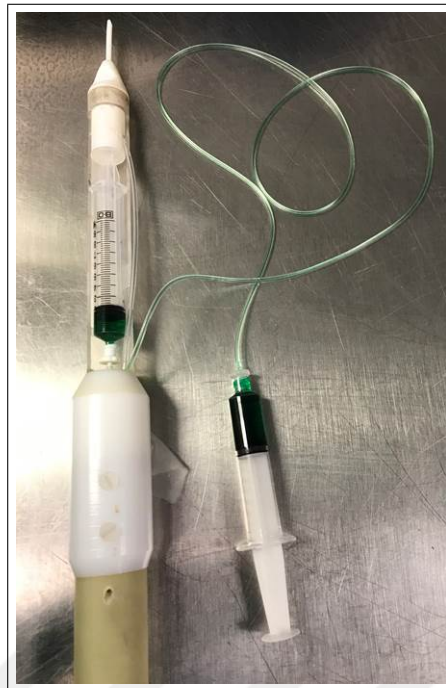


**Figure 3.1** A 10 cc syringe containing 1 mL of urease solution was placed in an animal bed and 3 cc of hyperpolarized sample was injected into the magnet with a connection line from out of the magnet, in order not to move the bed during scan.

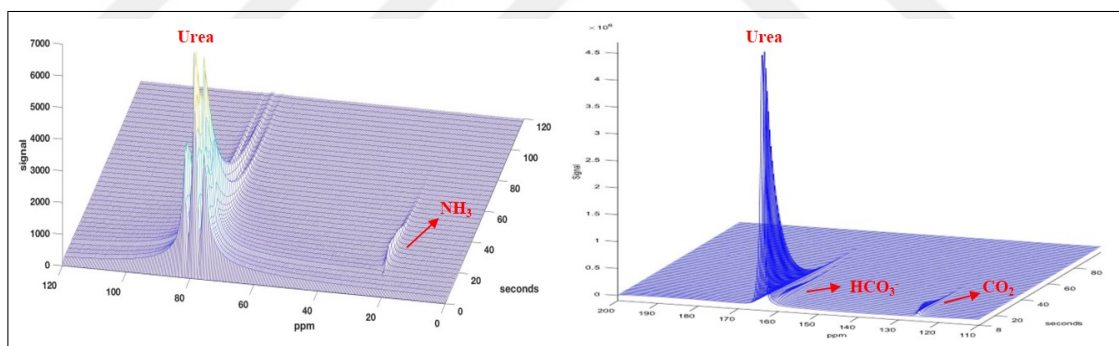


**Figure 3.2** (a) Conversion of HP  $^{15}\text{N}$  Urea to  $\text{NH}_3/\text{NH}_4^+$ .  $^{15}\text{N}/^1\text{H}$  30 mm Doty coil was used to acquire spectrum. (b) Conversion of HP  $^{13}\text{C}$  Urea to  $\text{CO}_2/\text{HCO}_3^-$ .  $^{13}\text{C}/^1\text{H}$  30 mm Doty coil was used to acquire spectrum. As expected,  $\text{CO}_2$  produced first and followed by  $\text{HCO}_3^-$ . Besides the ratio of  $\text{HCO}_3^-/\text{CO}_2$  gives the measure of pH.

## 3.2 Phosphorus-31 Magnetic Resonance Spectroscopic Imaging

Phosphorus-31 ( $^{31}\text{P}$ ) was the first non-invasive method for measuring tumor pH.  $^{31}\text{P}$  is 100% abundant and there are metabolites in the body contains phosphorus at concentrations up to 5 mM. As one of them inorganic phosphate ( $\text{P}_i$ ) has a pH sensitive chemical shift in the physiological range of pKa 6.8. Other peaks coming from

endogenous nucleoside triphosphates (NTP) and phosphocreatine (PCr) can be used as a reference since they do not have pH dependence [117]. Concentration of intracellular Pi is 2-3 mM while extracellular concentration is around 1 mM. Because of the higher volume fraction and higher concentration, signals containing Pi are recognized to be arising from intracellular compartment and reporting intracellular pH ( $\text{pH}_i$ ) [15], [118], [119], [117].

Several extracellular pH reporters have been developed for  $^{31}\text{P}$  MRS. Among these 3-aminopropylphosphonate (3-APP) has been widely used in vivo with its  $\text{pK}_a$  in the physiological range and being relatively insensitive to temperature and ion effect. This initially helped to report pHs from both extra- and intracellular compartments by using endogenous and exogenous molecules possess  $^{31}\text{P}$  [15]. It was followed with identifying the extracellular pH more acidic than normal tissue while intracellular pH is more alkaline. This identification opens doors to the studies targeting the acid-base pH gradient to treat cancer [109], [120], [121], [15].

### 3.2.1 $^{31}\text{P}$ MRSI of tumor microenvironment

For  $^{31}\text{P}$  MRS experiments an 8 mm surface  $^1\text{H}/^{31}\text{P}$  Doty coil was used. A calibration experiment was run in order to find the optimum power. The SPEC1d\_v2 image sequence with multiple experiments (different powers) provided by Bruker was used with a 100 mM 3-APP phantom. The optimum power (maximum signal) was obtained for  $^1\text{H}$  as 0.019W, for  $^{31}\text{P}$  as 0.068 W.

In order to determine tumor pH, a calibration curve was generated using phantoms contain 100 mM ATP and 100 mM 3-APP at different pHs at 37°C. Non-localized single-pulse sequences with a  $5^\circ$  pulse,  $\text{TR}=143.76$  ms, 1024 averages, and 2048 points were used to acquire  $^{31}\text{P}$  spectra. The calibration curve data were consistent with literature: the  $\text{pK}_a$ ,  $\delta_{\text{min}}$  and  $\delta_{\text{max}}$  were 7.0066, 21.225, and 24.807 respectively. Examples of spectra acquired from phantoms and calibration curve are given in (Figure 3.3).

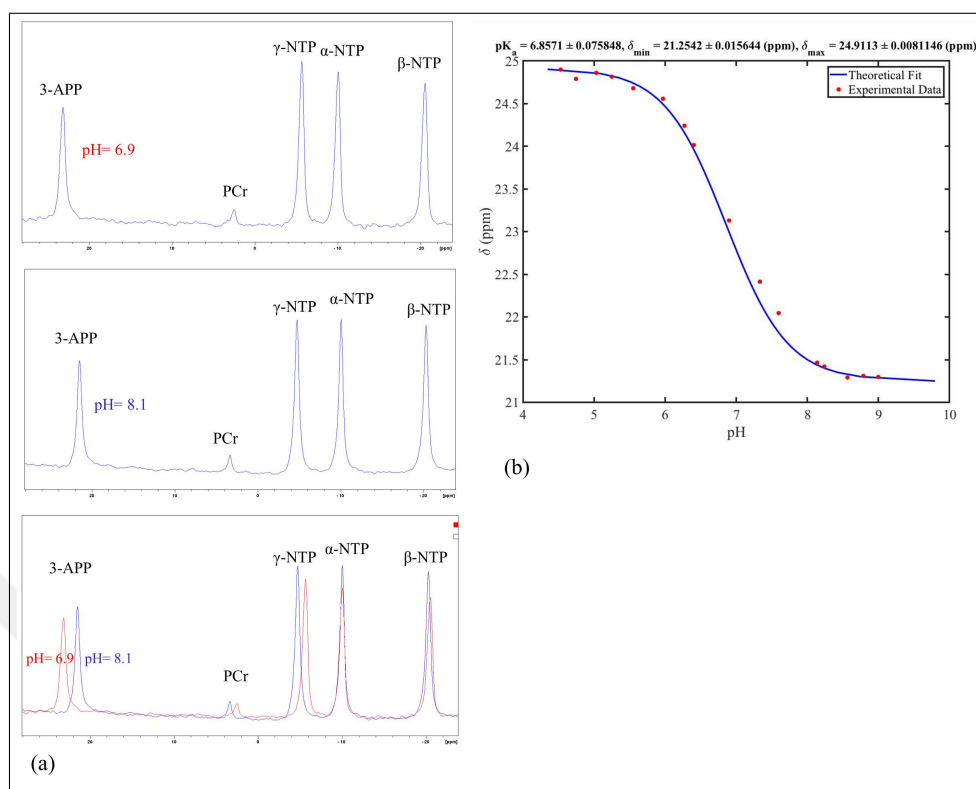


**Figure 3.3** (a) Spectra acquired from 3-APP phantoms.  $\alpha$ -NTP was used as a reference for 3-APP spectra and calibrated to have the peak at -10.05 ppm. (b) Calibration curve for 3-APP. Dots represent chemical shifts obtained from phantom spectra.

For in vivo pH measurement experiments NSG mice were injected with BxPC3 human pancreatic cancer cells which naturally express target of the drug, human CEA-CAM6 antigen. This expression was verified with flow cytometry (Figure 3.4).

Tumor pHs were determined with MRS of 3-APP following injection of 350  $\mu$ l of 500 mM 3-APP intraperitoneally (i.p.) 15 minutes before imaging. Mice were anesthetized for the duration of imaging with 1.5-2% isoflurane in oxygen. A fiber optic probe and a respiratory pad placed under the animal to monitor the temperature and respiration, respectively. The surface coil was placed at the top of the tumor and immobilized. Mice were placed into a 7T horizontal magnet (Agilent ASR 310; Santa Clara, CA) and (Bruker Biospin, Inc. BioSpec AV3HD; Billerica, MA) and position was adjusted to have the tumors into the isocenter of the magnet. Shimming was performed in terms of using the automated algorithms provided by Bruker then improved manually to achieve a line-width  $< 60$  Hz for water signal. After adjustments,



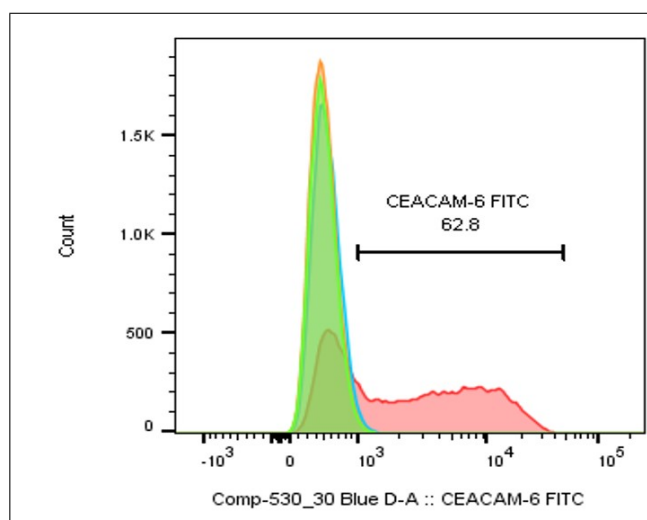


**Figure 3.4** Flow cytometry analysis for verification of CEACAM6 expression by BxPC3 cells.

a non-localized single-pulse sequences with a  $5^\circ$  pulse,  $TR=143.76$  ms, 4096 averages, and 2048 points were used to acquire  $^{31}P$  spectra. The  $\alpha$ -NTP peak was used as a reference at  $-10.05$  ppm. Tumor pHs were determined utilizing pH-dependent 3-APP peak. pH values were assigned based on the chemical shift of the contrast agent by corresponding this to calibration curve data. Mice with a tumor pH  $> 7$  were excluded from the study as a pilot data showed that alkaline range as baseline were unaffected by buffers or L-DOS47. 7 mice were injected with saline as controls while 9 mice were injected with  $90 \mu\text{g}/\text{kg}$  L-DOS47 intravenously (iv). Spectra were acquired 24 hours after each treatment as described previously. Examples of spectra for control and L-DOS47 injected mice are given in Figure 3.5.

Differences in pHs before and after treatments were calculated and compared for quantification purposes. The baseline average pHs were  $6.8 \pm 0.15$  and  $6.7 \pm 0.19$  for saline and L-DOS47 treatment groups, respectively. The differences of pHs before and after treatments for saline and L-DOS47 groups were statistically significantly different from each other (two tailed t-test,  $p=0.04$ ) as shown in Figure 3.6.

According to this data, L-DOS47 treatment resulted in alkalization of tumors that started with an acidic pH. The time course of pH responses can be used as a non-invasive measure of the pharmacodynamics (PD) of L-DOS47.

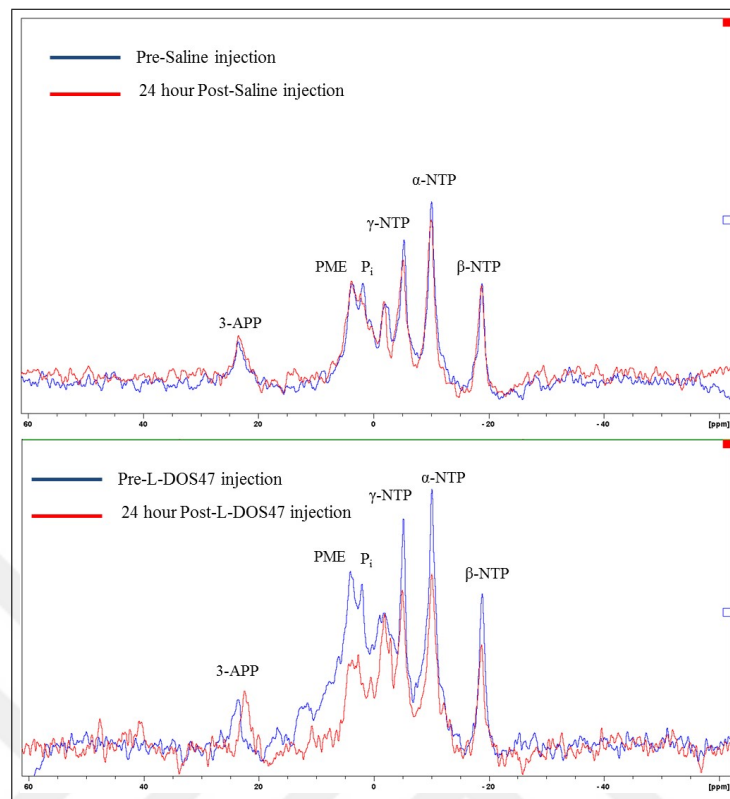


**Figure 3.5**  $^{31}\text{P}$  MRS of 3-APP for saline and L-DOS47 injected mice before and 24 hours after each treatment. As clearly seen from the figures 3-APP chemical shifts, which are pH dependent, fit into together for control mouse while the L-DOS47 injected one shows shifting to the right.

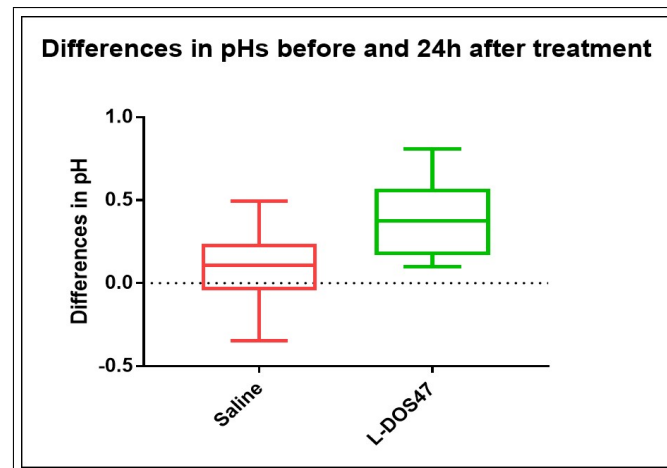


**Figure 3.6** The differences in tumor pHs for each mouse were determined before and 24 hours after saline/L-DOS47 treatments. The starting average pHs were  $6.8 \pm 0.15$  and  $6.7 \pm 0.19$  for saline and L-DOS47 treatment groups, respectively. Increase in tumor pH was higher for L-DOS47 injected mice ( $p < 0.05$ ).

### 3.3 Chemical Exchange Saturation Transfer (CEST) MRI

There are various techniques and contrast agents that have been suggested for being used to determine tumor pH by Magnetic Resonance Spectroscopic Imaging

(MRSI). The main disadvantage of spectroscopic methods is poor anatomic resolution caused by low sensitivity. CEST is a novel method can be used to determine pH in terms of using pH sensitive contrast agents with protons that are exchangeable with surrounding water molecules. The rates of such transfers, measured as a transfer of saturation can be pH dependent [122]. In this technique, when an RF pulse is applied, the protons in the contrast agent are weakened and transferred to water protons, causing a local deficiency in water signal [15]. Saturation can be transferred consecutively in terms of applying a series of pulses. A "Z- spectrum" is obtained by collecting the decreases in water signal intensity at selected frequencies as a function of RF pulses employed [15].

Computed Tomography (CT) has been utilizing the iodinated contrast agent, Iopamidol, for diagnosis for more than 30 years. It can be administered intravenously up to 400 mg/ml safely since it is soluble in water and has very low toxicity. Chemically, this molecule contains amide group protons that are in exchange with water [123]. Those amide protons resonate at 4.2 and 5.5 ppm with pH dependent exchange rates which provides a basis for establishing the ratiometric approach to determine pH. It has been verified that the range of pH can be measured accurately and precisely is 5.5 - 7.9 [124].

### 3.3.1 CEST of tumor microenvironment

A CEST imaging method for pH imaging was integrated to Moffitt Cancer Center Bruker 7T imaging spectrometer. pH calibration curve was obtained using 6 wells of a 96-well plate cut containing 20 mM of Isovue in phosphate buffered solution in the range of 5.9 - 7.2 (Figure 3.7).

Z-spectra acquired at 37 °C in terms of applying RF pulse to collect with a sustained wave presaturation block pulse at 3  $\mu$ T for 5 seconds by using  $^1\text{H}$  30 mm M2M coil. The saturation frequency offset was varied between 2.5 and -10 ppm with changing frequency resolutions to provide shorter acquisition times [122]. For anatomic

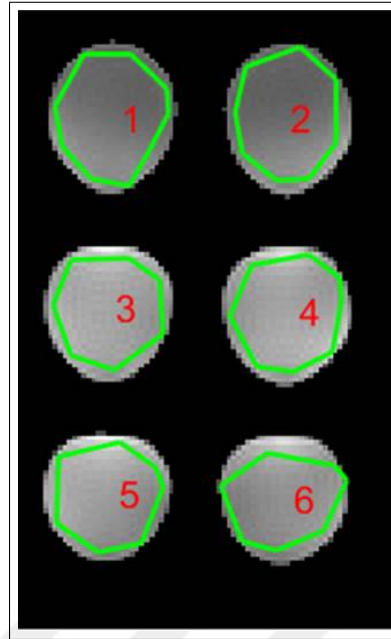


**Figure 3.7** T2 anatomical image of the phantom.

registration, coronal T2-weighted multislice (TE/TR = 31 ms/2271 ms, FOV = 80 x 30 mm<sup>2</sup>, matrix = 256 x 96, yielding in-plane resolution of 312  $\mu$ m and a slice thickness of 1.5 mm ) was acquired. CEST pH images were acquired using a TE/TR = 5.83 ms/ 6 s, with saturation bands of 3  $\mu$ T for 5 s, and a matrix = 171 x 64 over same FOV. CEST images were analyzed using MATLAB (The Mathworks, Inc., Natick, MA, USA). An intensity threshold filter was used in order to segment anatomical and Z-spectra images. The Z-spectra were interpolated voxel by voxel to place the bulk water to the right position, thus removing artifacts originating from B<sub>0</sub> inhomogeneity. The interpolated Z-spectrum was moved to the zero frequency for the bulk water resonance and the impact of Saturation Transfer (ST) was determined. In order to filter the noise, R<sup>2</sup> was calculated in terms of calculating signal-to-noise ratio of each voxel.

The threshold for R<sup>2</sup> was set to >0.99 for ST% and pH calculation [122].

In order to evaluate pH, the impacts of ST% were determined establishing a ratiometric procedure according to Eq. 3.1:

$$R_{ST} = ((100 - ST_{4.2\text{ppm}}))x(ST_{5.5\text{ppm}})/((100 - ST_{5.5\text{ppm}}))x(ST_{4.2\text{ppm}}) \quad (3.1)$$

$R_{ST}$  symbolizes the proportion of CEST at various pHs. Calibration curve is given in Figure 3.8.

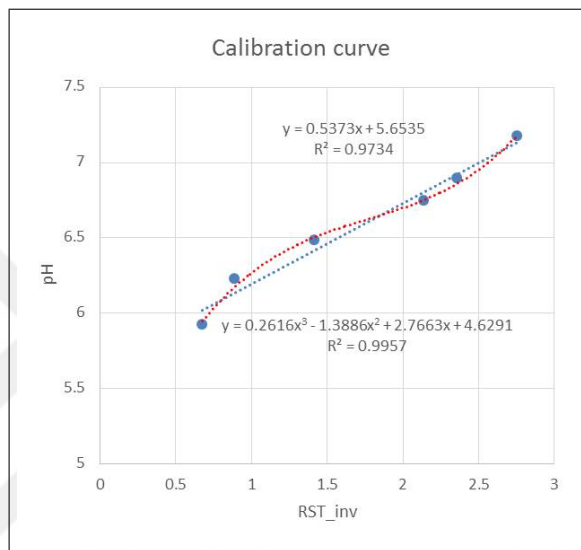


**Figure 3.8** Calibration curve for CEST of Iopamidol. Dots represent experimental data

In order to optimize the acquisition parameters (TE, TR, number of averages, etc.) and test the stability of system, several acquisitions were done with phantoms. As expected highest signal intensity was obtained with higher averages. However, signal intensity fluctuations were only around  $\sim 1\%$ . In order to eliminate any large variation in iopamidol concentration within the tumor, as well as any other change in physiological parameters or movement-related artifacts, parameters were used in order obtain the highest SNR with the shortest scanning time: which was TE/TR = 5.83 ms/ 6 sec, Average 1. Conditions and results for the stability test are given in (Figure 3.9).

After determining the optimum parameters, pH determination for mice have been started. Panc02 murine pancreatic adenocarcinoma cells were infected with human CEACAM6 lentivirus and expressing clones selected with puromycin. Binding

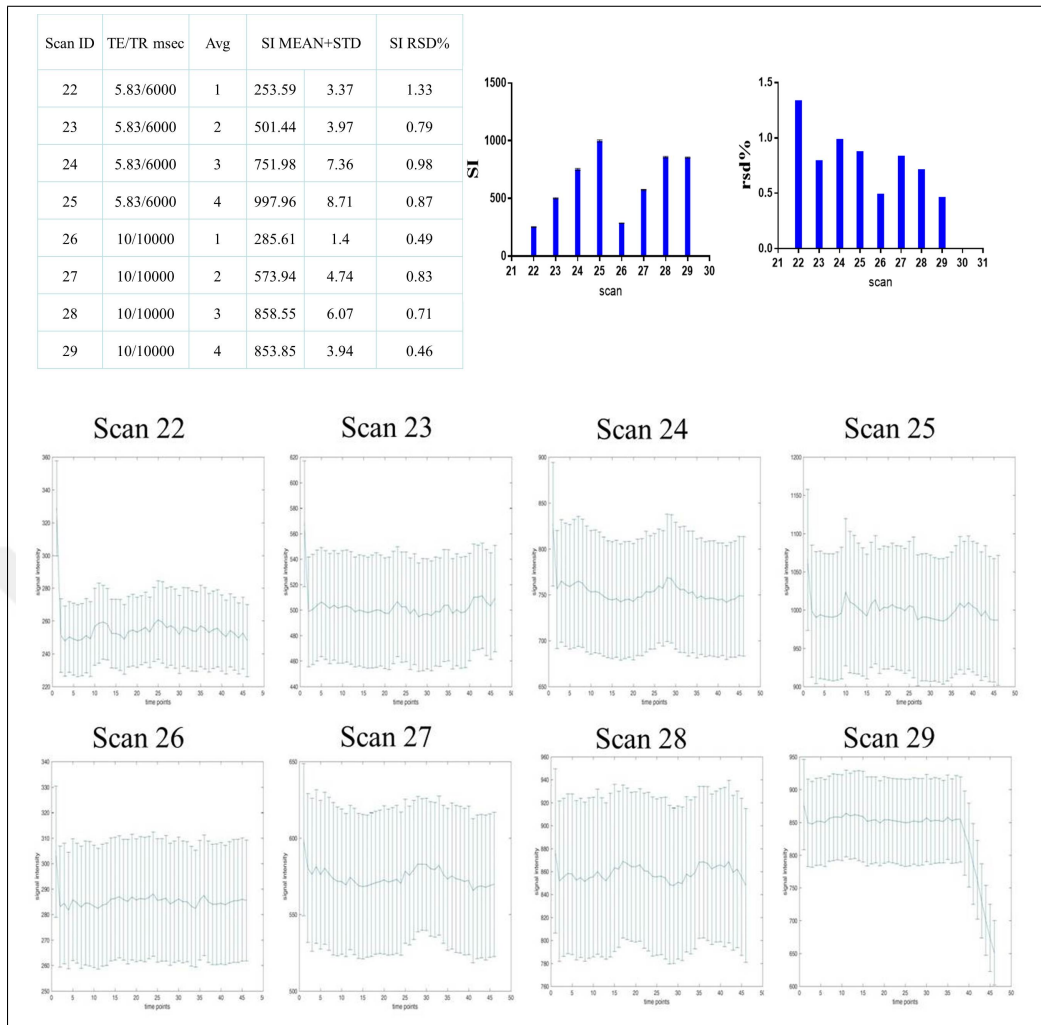


**Figure 3.9** Stability test with phantom for 8 different conditions. Signal intensity and standard deviations were calculated for each scan to determine the best parameters for in vivo imaging.

of L-DOS47 to Panc02 clone 38 cells were verified with flow cytometry (Figure 3.10). Infection and flow cytometry protocols will be given in detail in Chapter 3.

C57BL/6 mouse was subcutaneously inoculated with  $1 \times 10^6$  CEACAM6 Panc02 Clone 38 cells in the right flank and once tumor reached 500-700 mm<sup>3</sup> it was imaged with MRI Bruker 7T/MRI using Bruker 7T imaging spectrometer. Mouse was anesthetized for the duration of imaging with 1.5-2 % isoflurane in oxygen. A fiber optic probe and a respiratory pad were placed under the animal to monitor the temperature and respiration, respectively. A 30 mm <sup>1</sup>H M2M coil was used for CEST MRI.

For anatomic registration, axial T2-weighted multislice (TE/TR = 31 ms/1500

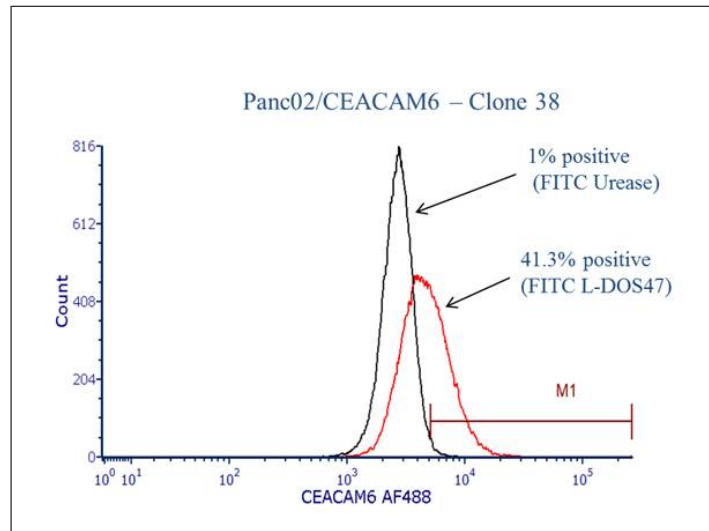


**Figure 3.10** Flow cytometry analysis for verification of CEACAM6 expression by Panc02 cells.

ms, FOV = 30 x 30 mm<sup>2</sup>, matrix = 128 x 128, slice thickness of 1.5 mm) was acquired. CEST pH images were acquired using a TE/TR = 5.83 ms/ 6 s, with saturation bands of 3  $\mu$ T for 5 s, and a matrix = 64 x 64 over same FOV. 350  $\mu$ l of contrast agent, Isovue, was injected subcutaneously (SC) next to the tumor and L-DOS47 was injected through iv catheter placed into the magnet with the mouse. As soon as pre-CEST was acquired 90  $\mu$ g/kg L-DOS47 was injected through the catheter and post image started to be acquired.

Tumor pHs were determined with respect to the evaluation of the  $R_{ST}$  values with the calibration pH-ratiometric data acquired from phantoms containing 20 mM Isovue (Figure 3.11).

Initially another C57BL/6 mouse was injected orthotopically (into pancreas) with 500000 CEACAM6 Panc02 Clone 38 cells in order to determine the effect of L-DOS47 an orthotopic model. An intravenous catheter was placed into the tail of the mouse to deliver Isovue and L-DOS47. Mouse was anesthetized for the duration of imaging with 1.5-2% isoflurane in oxygen. A fiber optic probe and a respiratory pad placed under the animal to monitor the temperature and respiration, respectively. For anatomic registration, coronal T2-weighted multislice (TE/TR = 31 ms/2271 ms, FOV

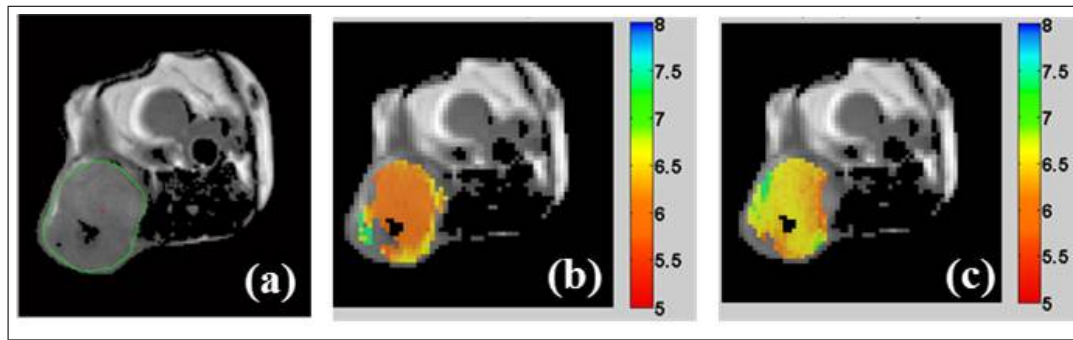


**Figure 3.11** CEST MRI of iopamidol for pH imaging of a Panc02 clone 38 SC tumor. (a) T2 weighted image, CEST MRI (b) before L-DOS47 injection, (c) 30 minutes after 90  $\mu\text{g}/\text{kg}$  L-DOS47 injection. L-DOS47 was administered iv while iopamidol was injected next to the tumor. M2M 30 mm  $^1\text{H}$  coil was used for the experiment.

= 80 x 30 mm<sup>2</sup>, matrix = 256 x 96, yielding in-plane resolution of 312  $\mu\text{m}$  and a slice thickness of 1.5 mm ) was acquired. CEST pH images were acquired using a TE/TR = 5.83 ms/ 6 s, with saturation bands of 3  $\mu\text{T}$  for 5 s, and a matrix = 171 x 64 over same FOV. An intravenous catheter was placed into mouse tail and connected to a syringe with a line in order to inject Isovue and L-DOS47 from outside the magnet without moving the animal bed. 350  $\mu\text{l}$  of contrast agent was injected iv for pre-CEST imaging. As soon as acquisition was completed 90  $\mu\text{g}/\text{kg}$  L-DOS47 was injected through the catheter and post image started to be acquired. In vivo pH values were estimated as described. As given in Figure 3.12, L-DOS47 was associated with alkalization of tumor pH for this model as well.



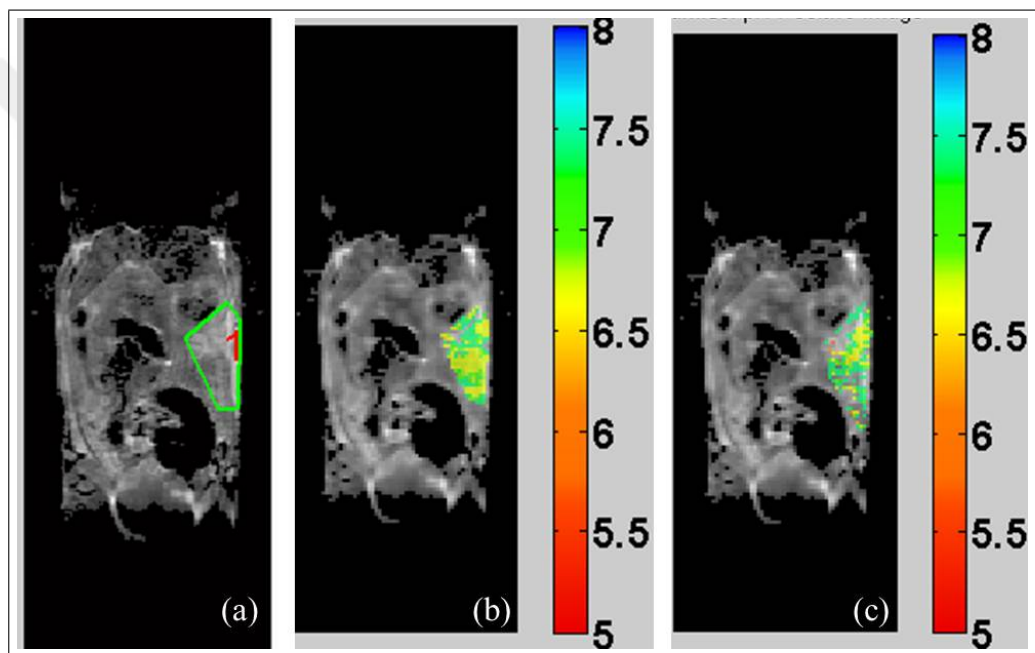


**Figure 3.12** CEST MRI of iopamidol for pH imaging of a Panc02 clone 38 orthotopic tumor. (a) T2 weighted image, CEST MRI (b) before L-DOS47 injection, (c) 30 minutes after 90  $\mu\text{g}/\text{kg}$  L-DOS47 injection. L-DOS47 and iopamidol were administered iv. M2M 30 mm  $^1\text{H}$  coil was used for the experiment.

## 4. TARGETING TUMOR MICROENVIRONMENT TO IMPROVE IMMUNOTHERAPY RESPONSES

### 4.1 Introduction

Resistance to therapy is critical in cancer prognosis. The acidic microenvironment of tumors have remarkable affect on efficacy of therapies including immunotherapy. Combined approaches with targeting tumor acidosis can improve clinical trial design and identify effective regimens to overcome treatment resistance [12].

The concept of neutralizing tumor acidosis improves treatment responses is not well-established yet, but recent study demonstrated that low pH is associated with inducing inflammatory cytokines [13]. T cells are not able to trigger off under acidic conditions because of the inflammatory signal initiation by acidic pH. Neutralizing tumor acidosis with buffer therapy may provide a basis to improvement of responses by boosting T cell activation.

In a previous study, mouse-bearing melanoma was treated with bicarbonate and an increase in tumor pH was observed. Bicarbonate therapy was combined with checkpoint inhibitors (PD-1/CTLA4). It was observed that, combination therapy significantly boosted the effects of these therapies [14]. Despite the promise for long-term consumption of alkaline buffers can be tolerated, the current clinical regimen cannot be prolonged in clinic as it requires ingestion of 40-50 (x 950 mg) capsules of  $\text{NaHCO}_3$  per day [125]. Indeed, three clinical trials of sodium bicarbonate failed due to poor patient compliance (NCT-1350583, NCT-01198821, and NCT- 1846429) which suggests investigation of new approaches to provide the same effect.

In this chapter, the effect of acidic tumor microenvironment on immunotherapy strategies was examined and targeting this stressor with L-DOS47 was combined with immunotherapy to improve the treatment outcomes.

#### 4.1.1 Microenvironment modifier drug: L-DOS47

Carcinoembryonic antigen-related cell adhesion molecule 6 (CEACAM6) is a member of human carcinoembryonic antigen (CEA) family. It was shown with several studies that CEACAM6 which is upregulated in several human cancers has a potential role in carcinogenesis and development [126]. A novel immunoconjugate (L-DOS47), targets the cell surface CEACAM6 antigens and urease part of the drug converts urea to ammonia was developed [102]. This increases the pH of the tumor microenvironment and alkalinizes the highly acidic environment that is needed for cancer cell survival and proliferation.

Antibody drug conjugates (ADCs) are composed of an antibody and a cytotoxic drug coupled via a bridging molecule. ADCs have advantage of binding to a specific site to the tumor and decreasing nonspecific side effects. The antibody part of the drug binds to the cell surface antigen enters to the cell and connector is split to liberate the cytotoxic drug. It is crucial to specify the tumor specific antigen, ADC must enter and connector must liberate the drug inside the cell.

Antibody directed enzyme prodrug therapy (ADEPT) utilizes a two-step approach. This technique charge the antibody-enzyme conjugates to the antigens at the tumor sites and eliminate the unbound conjugates from the bloodstream. When the accumulation is complete, a prodrug is administered and transformed to its cytotoxic form and fulfill the duty with selective tumor cell death.

L-DOS47 was developed with utilizing ADEPT approach with a modification of eliminating pro-drug administration. The drug contains a camelid antibody that binds to CEACAM6 antigens and a urease enzyme that hydrolyzes urea into ammonia to provide toxicity. This also increases tumor pH via urease enzyme, which converts urea to  $2 \text{ NH}_4^+$  and  $1 \text{ HCO}_3^-$  [102], [127].

### 4.1.2 Immunotherapy

The programmed cell death 1 receptor (PD-1) was discovered in the early 1990s and this discovery was followed by its identification of being a negative regulator of T cell responses when engaged with its ligand programmed death ligand 1 (PD-L1). In 2019, chimeric antigen receptor (CAR)-T cells and using checkpoint blockades for immunotherapy was announced by Science as Breakthrough of the Year [128], [129], and in 2018, the discoverer of PD-1 (Tasuku Honjo) was awarded the Nobel Prize in Physiology of Medicine.

T cell receptor (TCR) recognition by major histocompatibility complex (MHC) molecules initiates the generation of immunity by T cells. When T cells are activated they induce production of IFN- $\gamma$  which is recognized by IFN- $\gamma$  receptors in tumor microenvironment. This starts cascade of signals that eventually promotes PD-L1 expression by tumor cells which prevents further T-cell mediated killing. Blocking the interaction between anti PD-1 and PD-L1 promotes T cell persistence resulting in enhanced cytotoxic T cell response [128].

Anti-tumor immunity is inhibited by several factors including expression of checkpoint inhibitors, infiltration of inhibitory cells such as myeloid derived suppressor and regulatory T cells (MDSCs, Tregs) and secretion of inhibitory factors. As described in the first chapter, the acidic microenvironment of tumors can also blunt anti-tumor T cell responses in terms of inhibiting effector T cells. Blockade of PD1 [130], and/or CTLA4 [131] with monoclonal antibodies has led to durable anti-tumor responses in patients where conventional therapies have failed [132], [133]. However, only 20 - 25 % of patients with non-small-cell lung cancer, melanoma, or renal-cell cancer were responded to anti-PD1 treatment [134], and the response rate to anti-CTLA-4 is 11%. Combining both checkpoint inhibitors resulted in a 40% response rate [135]. While this is an improvement, it also means that 60% of patients receive no benefit, suggesting that there should be alternative approaches (such as increasing pH) to boost therapy responses.

## 4.2 Generation of Cancer Model to be Used for the Study

Immunocompetent mice were required to test the effects of L-DOS47 in combination with immunotherapy. As human tumors will be rejected by immunocompetent mice, mouse tumor models needed to be generated. Since mouse cells do not express CEACAM6 and are thus not targets for L-DOS47, LKR murine lung and Panc02 murine pancreatic cancer cells, were retrovirally infected with human CEACAM6, the target of the drug.

### 4.2.1 LKR/CEACAM6 preclinical model

#### Mice

All mice were housed in the animal facility at Moffitt Cancer Center. 129S4/SvJaeJ mice were obtained from Jackson Laboratories. Mice were sacrificed if tumor volume went beyond 2000 mm<sup>3</sup> or showed serious ulcerations based on American Veterinary Medical Association Guidelines by exposing of CO<sub>2</sub>. Institutional Animal Care and Use Committee (IACUC) was reviewed and approved all techniques and procedures used for animal experiments based upon U.S. Public Health Service Policy and National Research Council Guidelines.

#### Retroviral infection of LKR murine lung cells

3 wells of a 24-well plate were plated with 80000 cells/well to have 50% cell density at the day of infection. In order to increase infection efficacy complete media with a concentration of 8 µg/ml Polyberene was used. 10 µl of viruses for blank and CEACAM6 vectors were added to the corresponding wells. The 3<sup>rd</sup> well was used as a control. Next day fresh media with 1 µg/ml puromycin was added to each well. After the selection, individual single clones were transferred to individual wells in a 24-well plate. When they grew, were split to 6-well plates. Real Time Reverse Transcription

Polymerase Chain Reaction (RT-PCR) and flow cytometry were done to determine the presence of antigen of interest.

### Verification of CEACAM6 expression on infected LKR murine lung cells

RNeasy kit was used for RNA purification from LKR clones. As a preparation for RT-PCR experiments, cDNA was obtained by mixing 4  $\mu$ l iscript, 1000 ng RNA with water to have 20  $\mu$ l of final volume in terms of using the program prepared for it. Following that step, RT-PCR experiment was set up for each clone as shown in Figure 4.1. Since mouse cell line was used, a mouse reference gene was used as control. Two separate master mix was prepared as one for CEACAM6 primers, one for m18sRNA (reference mouse gene).

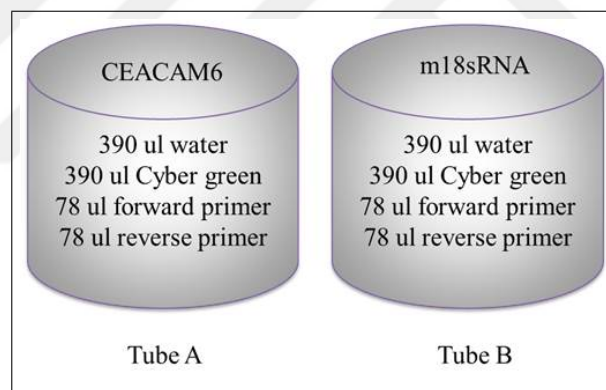


**Figure 4.1** Master mix preparation for RT-PCR.

20  $\mu$ l of master mix was aliquoted to each well (96 well plate for RT PCR). In each well 2.5  $\mu$ l of cDNA from clones were added. Plate was covered with film and spun down. Program was run for TA: 52 °C. Melting curves are given in Figure 4.2 for clones.

As seen from data, there is a difference with Clone 13 in the melting curve. A gel was run with PCR products for LKR parental cells, empty vector infected cells, Clones #2, #7, #13, and #14. According to literature [136] it is expected to see the band on 353 bp for CEACAM6. A gel image is shown in Figure 4.3.

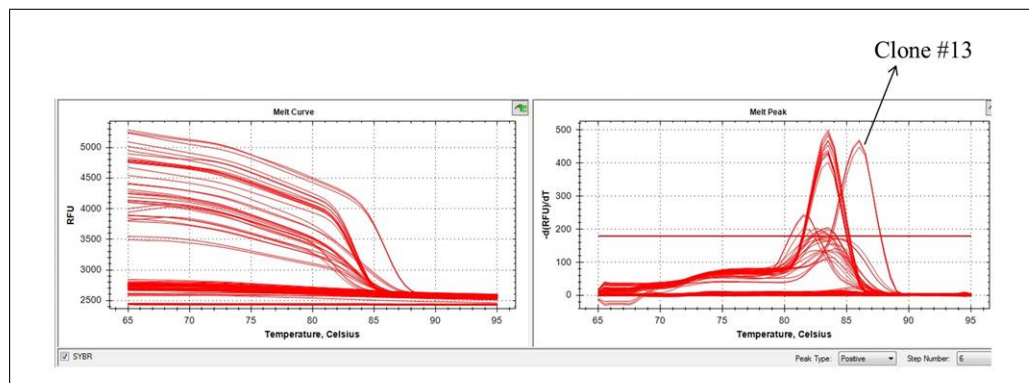


**Figure 4.2** Melting curves for RT-PCR experiment.

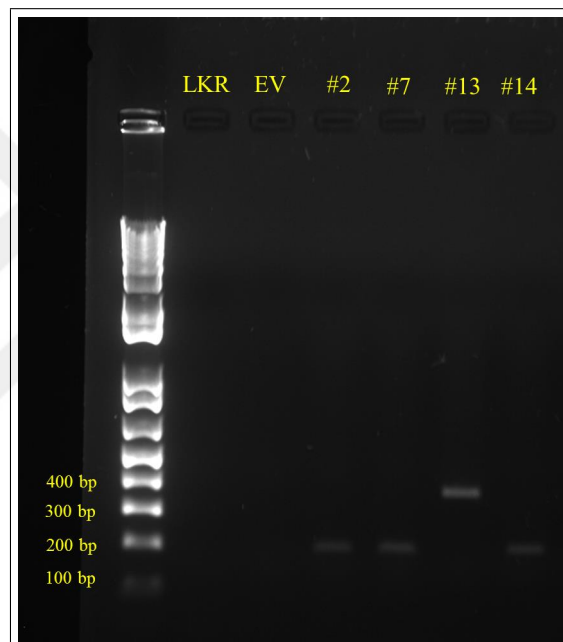


**Figure 4.3** Gel image for PCR products.

Gel showed that # 13 could be a good clone, have high chance of expressing the target.

This expression was also verified with flow cytometry in terms of using a 3-step staining protocol. LKR Clone 13 and parental LKR cells were stained either with L-DOS47 ( $\mu\text{g}/\text{ml}$ ) or Urease (for negative control) and incubated on ice for half an hour at the first step and then washed 3 times with staining buffer (DPBS with 2% Feval Bovine Serum) for 3 times. Then they were stained with ( $5.8 \mu\text{g}/\text{ml}$ ) anti-urease and ( $1.5 \mu\text{g}/\text{ml}$ ) AF488, respectively for detection. Samples were fixed with 1%

Paraformaldehyde (PFA), stored in 4°C and analyzed with Canto flow cytometer the next day. Results are given in Figure 4.4.

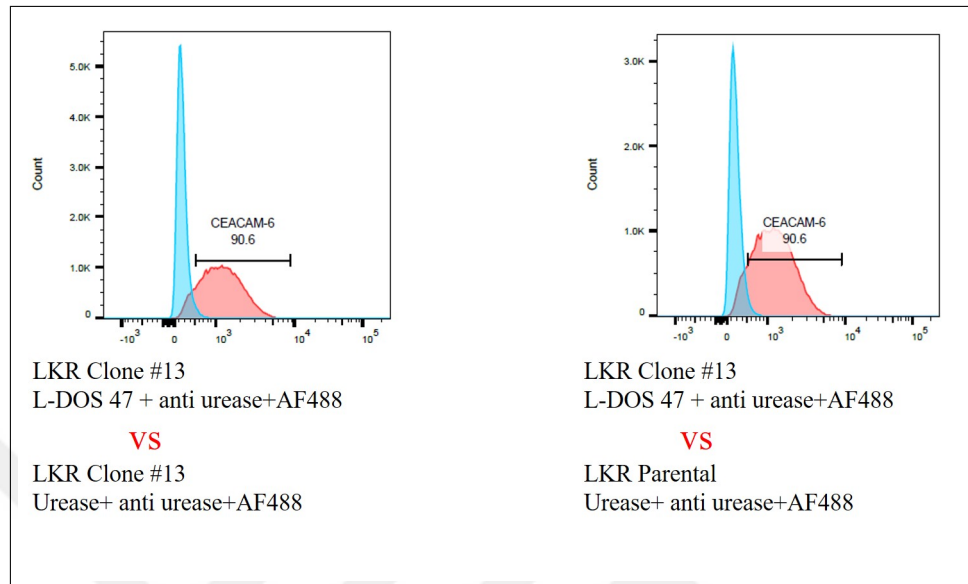


**Figure 4.4** LKR parental and Clone 13 Cells were stained with Urease/ L-DOS47 as negative and positive controls respectively. CEACAM6 expression for LKR clone was verified to be 90% with flow cytometry.

### L-DOS47/Anti-PD-1 combination for LKR/CEACAM6 preclinical model

In order to determine the boosting effect of L-DOS47 when combined with anti-PD1, 30 129S4/SvJaeJ mice (1 million cells/mouse) were inoculated with LKR Clone # 13 subcutaneously in the right flank. They were randomized into 5 groups (Bicarbonate + Anti-PD1, L-DOS47, L-DOS47 + Anti-PD1, IgG, Anti-PD1). Bicarbonate treatment was started 3 days before tumor injection. Doses were as the following: L-DOS47: 87.5  $\mu$ /kg; anti-PD1: 300  $\mu$ g/mouse; IgG: 300  $\mu$ g/mouse; Bicarb: 200 mmol/L (in drinking water). Mice received 4 doses of each treatment in total. When experiment was terminated, according to the tumor volume measurements, anti-PD1 alone was able to have a complete response in most of the mice and there were regressions even in control group (Figure 4.5). It was concluded that addition of human CEACAM6 to LKR cells affected the tumor and resulted with regression. This model cannot be used.



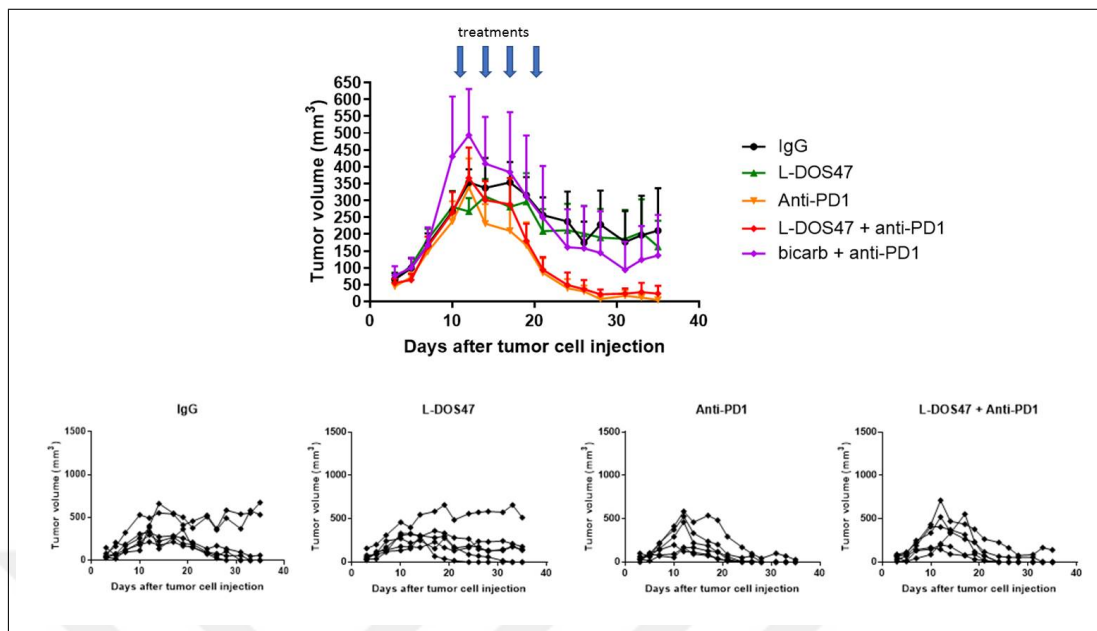


**Figure 4.5** Average and individual volumes for 129S4/SvJaeJ mice injected with LKR Clone 13 cells. 13 days after tumor inoculation, regression in tumor growth in all groups was observed. As seen from data for individual mice, there were mice with complete response in all groups.

#### 4.2.2 Panc02/CEACAM6 preclinical model

##### Mice

C57BL/6 female mice were purchased from Jackson Laboratories and housed in the animal facility at Moffitt Cancer Center under specific pathogen-free conditions. Mice were sacrificed if tumor volume went beyond 2000 mm<sup>3</sup> or showed serious ulcerations based on American Veterinary Medical Association Guidelines by exposing of CO<sub>2</sub>. Institutional Animal Care and Use Committee (IACUC) was reviewed and approved all techniques and procedures used for animal experiments based upon U.S. Public Health Service Policy and National Research Council Guidelines.

##### Retroviral infection of Panc02 murine pancreatic cells

3 wells of a 24-well plate was plated with 80000 Panc02 mouse pancreatic cancer cells/well to have 50% cell density at the day of infection. In order to increase infection

efficacy complete media with a concentration of 8  $\mu\text{g}/\text{ml}$  Polyberene was used. 10  $\mu\text{l}$  of viruses for blank and CEACAM6 vectors were added to the wells. The 3<sup>rd</sup> well was used as a control. Next day fresh media with 8  $\mu\text{g}/\text{ml}$  puromycin was added to each well. After the selection, every clone (single cell origin) was transferred to 24-well plate. When they grew, were split to 6-well plates. The workflow is given in Figure 4.6.

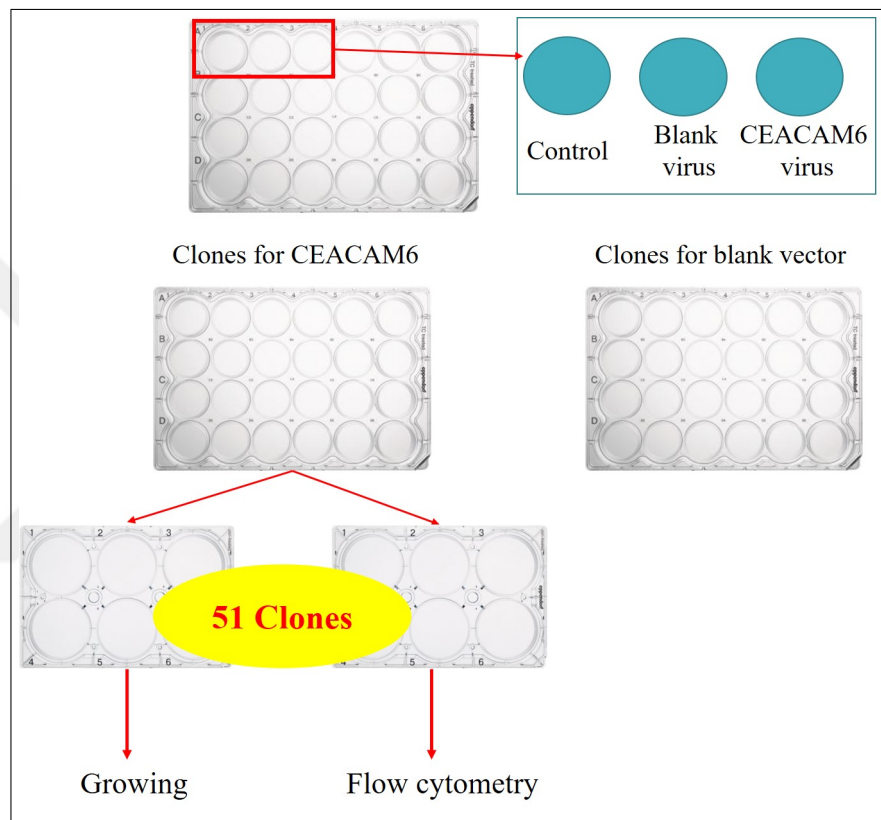


**Figure 4.6** Workflow for infection experiments in order to provide expression of CEACAM6 antigen.

Expression was verified with flow cytometry in terms of using a FITC labelled L-DOS47. BxPC3 human pancreatic cancer cells and Panc02 parental cells were used as positive and negative controls, respectively. All cells were stained with 5 $\mu\text{g}/\text{ml}$  FITC labelled L-DOS47 in a V-bottom 96-well plate, incubated on ice for 30 minute then washed for 3 times with staining buffer. Samples were fixed in terms of using 1 % PFA and stored in 4°C. Experiment was run on next day with IQue flow cytometer. 51 clones were screened for expression, results are given in Figure 4.7.

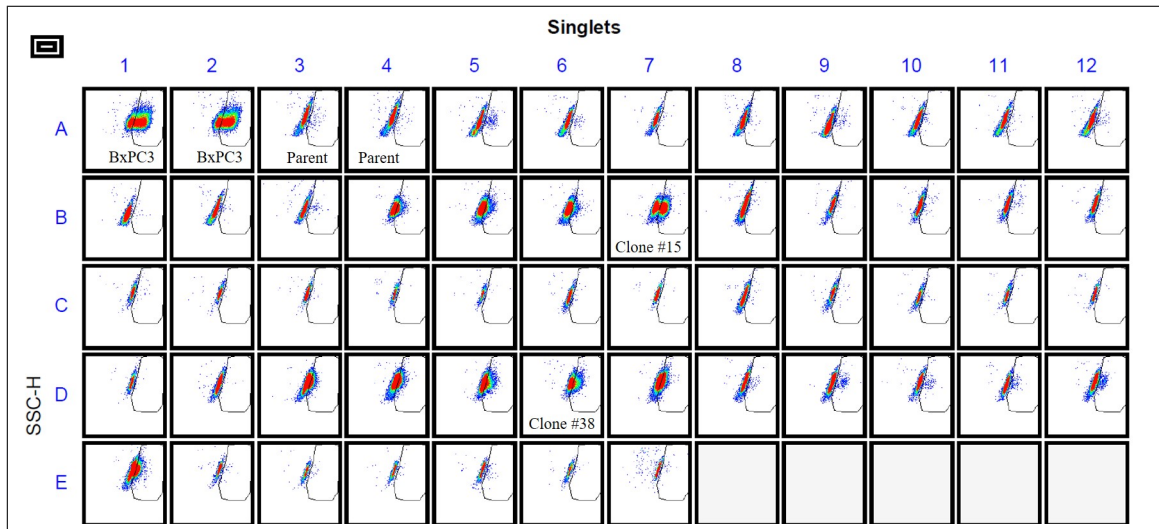


**Figure 4.7** CEACAM6 expression for Panc02 clones were verified with flow cytometry.

Since in previous experiment regression in tumor growth was observed, 4 mice were inoculated with Panc02 CEACAM6 clone 38 (1 million cells/mouse) and one with parental Panc02 cells (1 million cells/mouse) subcutaneously (SC) into right flank of C57BL/6 mice. Tumor growth was followed for 15 days and no sign for regression was observed. Tumor volumes are given in Figure 4.8.

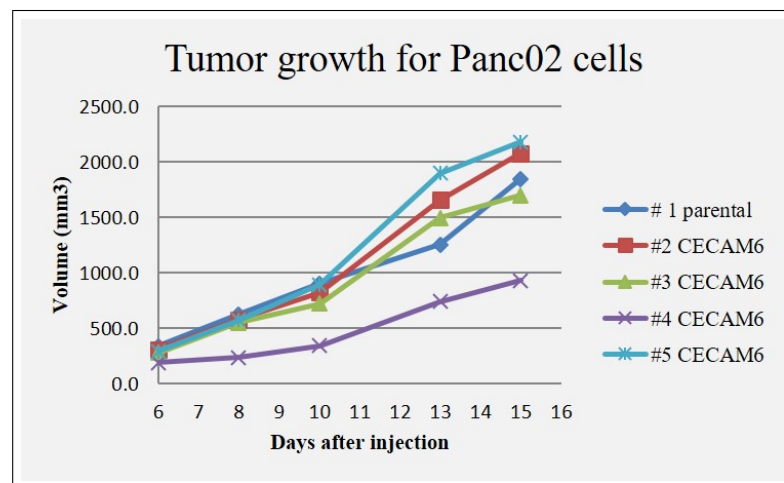


**Figure 4.8** Comparison of tumor growth for Panc02 Parental and CEACAM6 expressing clone (Clone 38) injected mice. Regression was not observed in tumor growth for this model.

### L-DOS47 titration experiment for Panc02/CEACAM6 preclinical model

An experiment was designed with two different clones have different expression patterns. Clone 15 has bi-distribution (small but well differentiated population expressing CEACAM6), Clone 38 has the highest percent of binding for CEACAM6. L-DOS47 was also titrated -in vivo- in this experiment. Comparison of expressions for the clones are given in Figure 4.9.

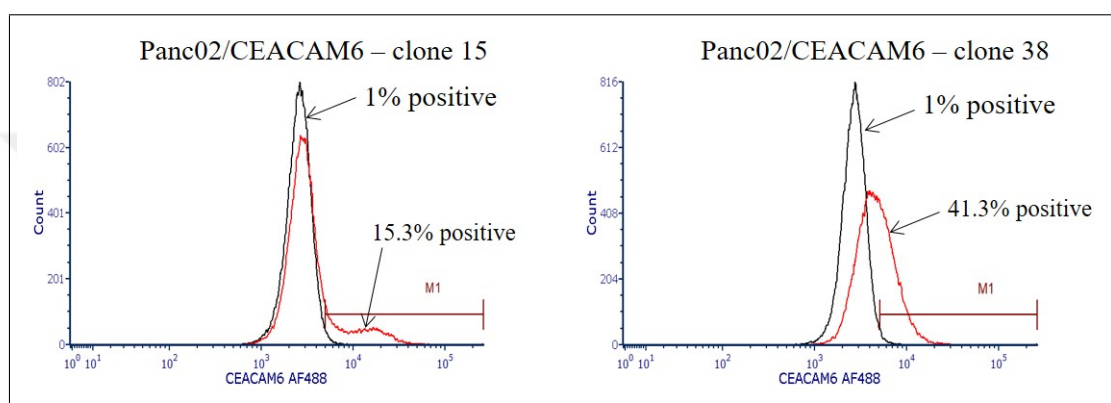


**Figure 4.9** Flow cytometry analysis for Panc02 parental, CEACAM6 15 and 38 clones.

$1 \times 10^6$  CEACAM6 Panc02 Clone 15 or Clone 38 cells were injected subcutaneously in the right flank of  $20 + 20$  C57BL/6 mice. On the 4<sup>th</sup> day after tumor injection mice were randomized into 4 groups as: Saline, L-DOS47 ( $10 \mu\text{g}/\text{kg}$ ), L-DOS47 ( $30 \mu\text{g}/\text{kg}$ ), L-DOS47 ( $90 \mu\text{g}/\text{kg}$ ). Treatments were given on 4<sup>th</sup>, 7<sup>th</sup>, 10<sup>th</sup> and 13<sup>th</sup> they after tumor cell injections intravenously (iv). Average tumor volumes for each group is given in Figure 4.10. According to volume measurements it was shown that effects for  $30 \mu\text{g}/\text{kg}$  and  $90 \mu\text{g}/\text{kg}$  doses were similar while  $10 \mu\text{g}/\text{kg}$  was showing slight effects.  $90 \mu\text{g}/\text{kg}$  for dose of L-DOS47 and Clone 38 were chosen to be used for in vivo experiments going forward.

### L-DOS47/Anti-PD1 combination for Panc02/CEACAM6 preclinical model

$1 \times 10^6$   $20$  C57BL/6 mice were inoculated with CEACAM6 Panc02 Clone 38 cells in the right flank. On the 4<sup>th</sup> day after tumor injection mice were randomized into

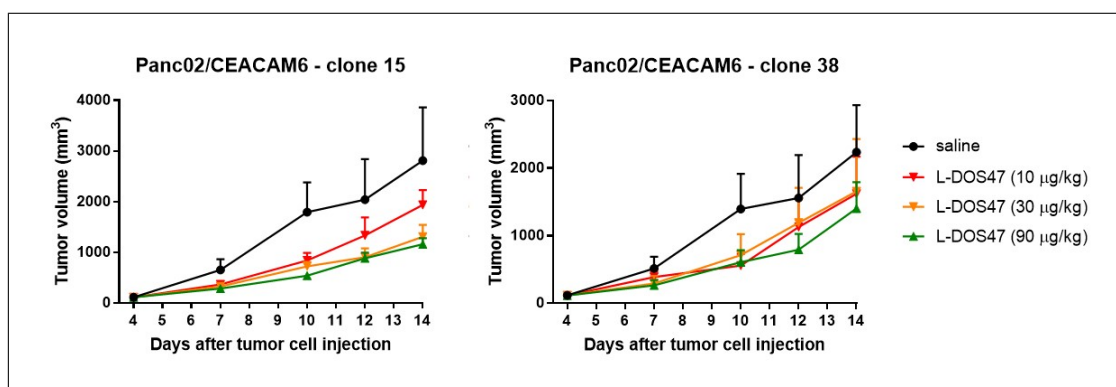


**Figure 4.10** In-vivo titration of L-DOS47 for Panc02 Clone 15 and Clone 38 injected mice. Results have shown that Panc02 clone 15 and clone 38 responded similarly to L-DOS47 therapy.

4 groups as: Saline, L-DOS47 (90  $\mu\text{g}/\text{kg}$ ), anti-PD1 (300  $\mu\text{g}/\text{mouse}$ ) and L-DOS47 (90  $\mu\text{g}/\text{kg}$ ) + anti-PD1 (300  $\mu\text{g}/\text{mouse}$ ). Treatments were given on 4<sup>th</sup>, 7<sup>th</sup>, 10<sup>th</sup> and 13<sup>th</sup> day after tumor cell injections intravenously (iv) for saline and L-DOS47, ip for anti-PD1 treatments. Mice were sacrificed after the last dose. Average and individual tumor volumes for each group are given in Figure 4.11. While there was a big variation among mice especially in saline group, average tumor volume and standard deviation was tight for combination group. Results were encouraging and it was concluded that L-DOS47 addition before anti-PD1 treatment helps to improve immunotherapy responses.

12 male and 12 female C57BL/6 mice were purchased from Jackson Laboratories and housed at the Animal Research Facility of the H. Lee Moffitt Cancer Center and Research Institute (Tampa, FL) to start a breeding colony. Combination experiment was repeated two times with the mice from the colony with mixed genders. For next two combination experiments 10 mice/ group (5 males + 5 females) were used in order to provide statistically significant results. 40 C57BL/6 mice were inoculated with CEACAM6 Panc02 Clone 38 cells in the right flank. On the 4<sup>th</sup> day after tumor injection mice were randomized into 4 groups as: Saline, L-DOS47 (90  $\mu\text{g}/\text{kg}$ ), anti-PD1 (300  $\mu\text{g}/\text{mouse}$ ) and L-DOS47 (90  $\mu\text{g}/\text{kg}$ ) + anti-PD1 (300  $\mu\text{g}/\text{mouse}$ ). Treatments were given on 4<sup>th</sup>, 7<sup>th</sup>, 10<sup>th</sup> and 13<sup>th</sup> day after tumor cell injections intravenously (iv) for saline and L-DOS47, ip for anti-PD1 treatments. In those experiments mice were followed until endpoint (2000  $\text{mm}^3$  in tumor volume or serious ulceration) in order to follow survivals. It was observed that survivals of the mice in combination therapy

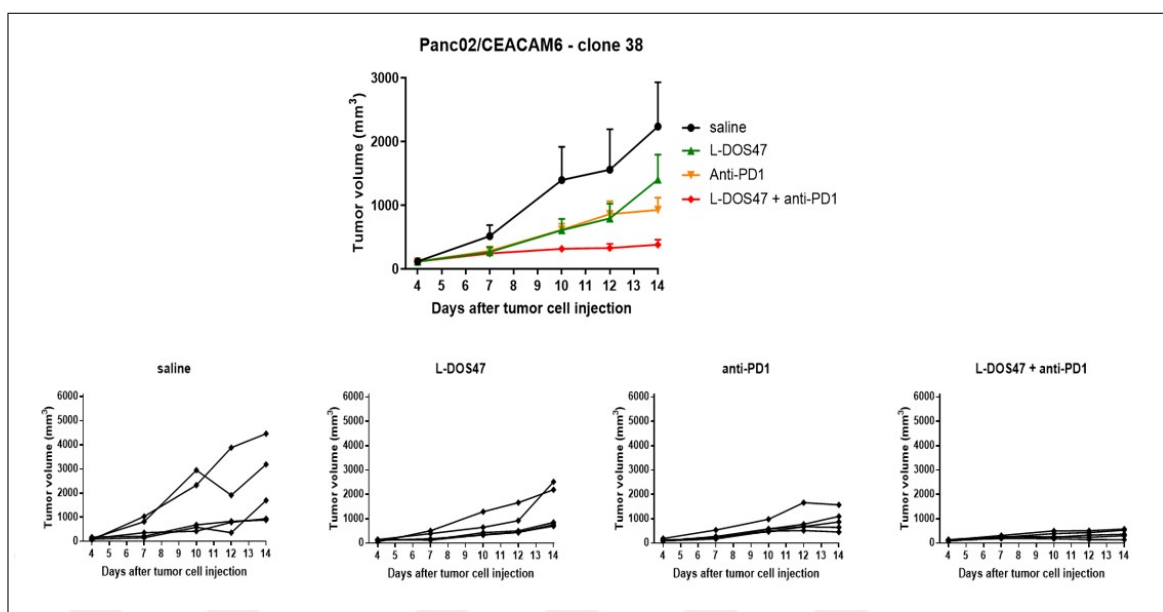


**Figure 4.11** Average and individual tumor volumes for mice in each group (Saline, L-DOS47, Anti-PD1 and combination.) Addition of L-DOS47 to anti-PD1 treatment boosted the effect of immunotherapy on tumor growth.

group was longer than any other treatment groups. However, a slow growth pattern and anti-PD1 sensitivity were observed in those combination experiments for a few mice as well. In order to investigate this, an *in vivo* titration experiment for anti-PD1 was designed.

40 C57BL/6 mice were inoculated with  $1 \times 10^6$  CEACAM6 Panc02 Clone 38 cells in the right flank, subcutaneously. Four days later tumor sizes were measured with caliper and mice were forcibly randomized to groups to have the same average tumor size in each group. Groups were as following: Anti-PD1 15  $\mu\text{g}/\text{kg}$ -twice a week, Anti-PD1 5  $\mu\text{g}/\text{kg}$ -twice a week, Anti-PD1 1.7  $\mu\text{g}/\text{kg}$ -twice a week, Anti-PD1 15  $\mu\text{g}/\text{kg}$ -once a week and saline. Average tumor volumes for each group and the last day tumor measurements are given in Figure 4.12. As seen from the tumor volumes 15  $\mu\text{g}/\text{kg}$  twice a week group received the most effective treatment and followed by others. Based on this data, the dose for anti-PD1 treatment reduced to 5  $\mu\text{g}/\text{kg}$  for further experiments.

Another experiment was designed to compare the sensitivities of Panc02 Parental, Clone 15 and Clone 38 cells to anti-PD1 treatment. Since a foreign protein inserted

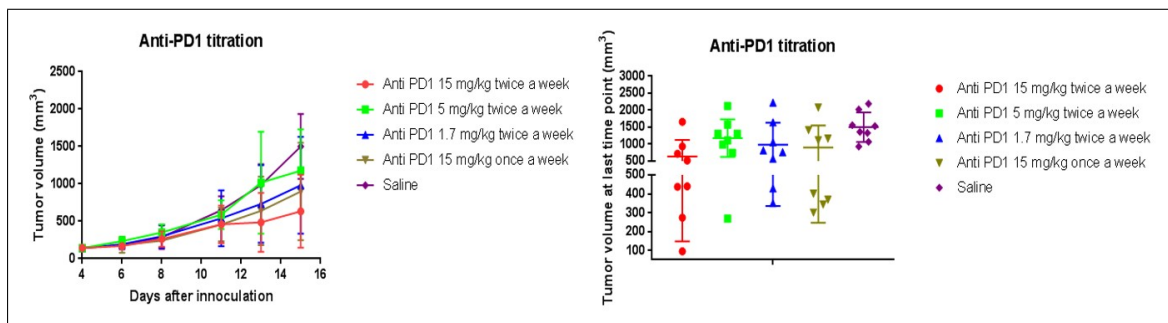


**Figure 4.12** Average tumor volumes for entire experiment and at endpoint with respect to different doses of anti-PD1. 15  $\mu\text{g}/\text{kg}$  twice a week is the most effective followed by 15  $\mu\text{g}/\text{kg}$  once a week. Interestingly 1.7  $\mu\text{g}/\text{kg}$  group was more effective than 5  $\mu\text{g}/\text{kg}$  group.

to cells it was tested that if this affected the sensitivity to anti-PD1. Two clones were chosen with different CEACAM6 expression levels and patterns (Figure 4.13) and compared with Panc02 parental cells. 14 mice (mixed genders) were injected with each cell line and each cell line was divided into two groups as anti-PD1 (5  $\mu\text{g}/\text{kg}$ ) and saline. Treatments were started 4 days after tumor inoculation and continued to be given on 7<sup>th</sup>, 10<sup>th</sup> and 13<sup>th</sup> days. Average tumor volumes for each group and the last day tumor measurements are given in Figure 4.14. Based on these data it was confirmed that Panc02 Clone 38 cells can be continued to use further experiments as tumors were growing faster and no sensitivity was observed to anti-PD1 treatment.

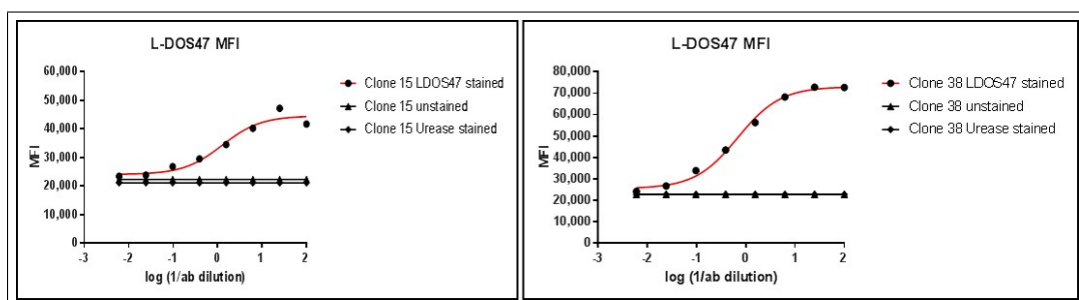


**Figure 4.13** Flow cytometry analysis for Panc02 Parental, Clone 38 and Clone15 cells to determine CEACAM6 expression.

The fourth immunotherapy combination experiment designed with 12 mice/group (6 females + 6males) and reduced the dose of anti-PD1 to 5 mg/kg. Groups were as following: Saline, L-DOS47 (90  $\mu\text{g}/\text{kg}$ ), anti-PD1 (5mg/kg) and L-DOS47 (90  $\mu\text{g}/\text{kg}$ ) + anti-PD1 (5 mg/kg). Treatments were given on 4<sup>th</sup>, 7<sup>th</sup>, 10<sup>th</sup> and 13<sup>th</sup> day after tumor

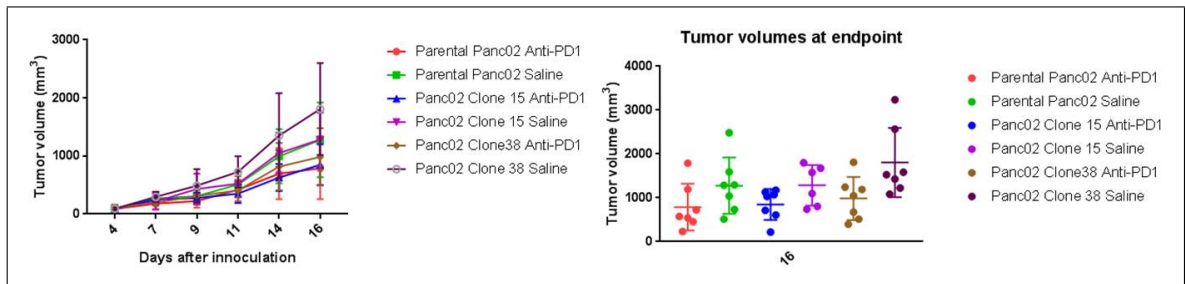


**Figure 4.14** Average tumor volumes for entire experiment and at endpoint for saline and anti-PD1 treated mice injected with either Clones 15/38 and parental Panc02 cells. Tumors were growing faster for Panc02 Clone 38 cells injected mice for both anti-PD1 and saline treated groups compared to Panc02 Parental and Clone15 cells.

cell injections; intravenously (iv) for saline and L-DOS47, ip for anti-PD1 treatments. Mice were sacrificed when they reached to endpoint ( $2000 \text{ mm}^3$  in tumor volume or had serious ulcerations). They were followed until endpoints in order to obtain survival information.

After the completion of all four experiments, survival days of all mice for each group are gathered together and Kaplan Meier curve was generated Figure 4.15. 148 mice were included to study in total and each group (L-DOS47, anti-PD1, saline and combination groups) had 37 mice. It was shown that L-DOS47 addition was resulted with increase in survival for when used with anti-PD1 treatment.



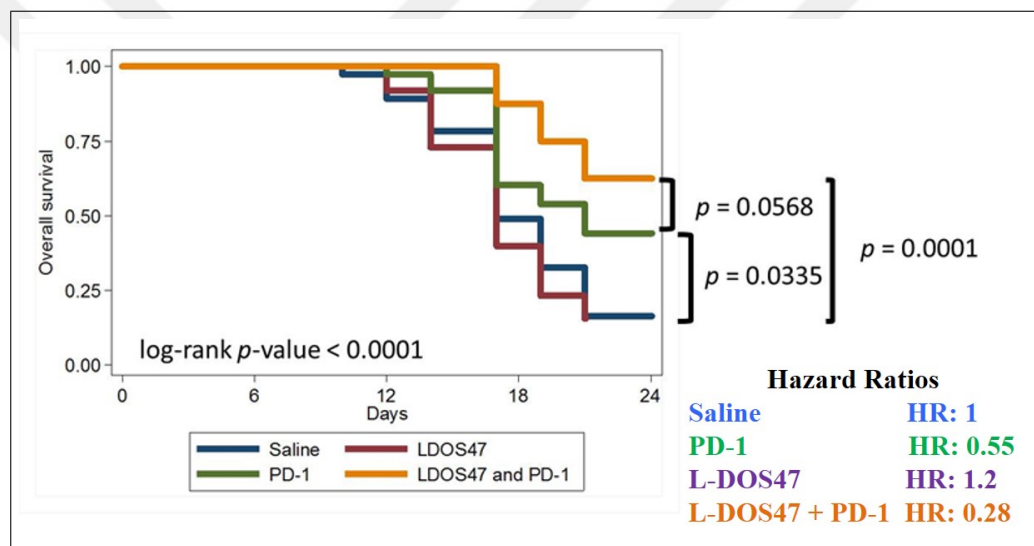


**Figure 4.15** Kaplan Meier curve generated for 4 in vivo L-DOS47 & anti-PD1 combination experiments. The  $p$  value was determined as 0.0001 for the difference in survival between combination and saline groups. This value was 0.0568 for the difference between combination and anti-PD1 groups.

## 5. OVERALL CONCLUSIONS

The main concentration in cancer biology and therapy has been on genetic and epigenetic remodelling in malignant cells [137]. However, it has been understood that tumor cells do not act alone and has close interaction with extracellular matrix which has remarkable affect on cancer progression and support almost all of the hallmarks of cancer [19], [1].

Notably, cancer cells rely on glycolysis even if oxygen is available. This phenomenon is called aerobic glycolysis or the Warburg effect [138]. This is paradoxical, as fermenting glucose yields 2 ATP molecules per glucose, whereas complete oxidation of glucose yields 36 ATP molecules. This altered energy metabolism is identified as one of the "hallmarks of cancer" [1]. Glycolysis occurs more rapid compared to oxidative phosphorylation. Increased ATP production rate is being considered responsible to facilitate proliferation of cancer cells [103]. For all these reasons, it can be inferred that cancer cells will be huge users of glucose to provide their energy. High glycolysis rates in cancer cells result in lactate overproduction. As cancer cells export lactate rather than using as a nutrient, it acidifies the tumor microenvironment [105].

Tumor-derived acidosis has been shown to suppress immune function [10]. Recent studies demonstrate that acidosis can alter the functions of cells of the immune system including T cells, neutrophils, macrophages and DC's [23], [77]. In a previous in vivo experimental study with mice bearing melanoma, tumor pH was neutralized with bicarbonate and combined with checkpoint inhibitors (PD-1/CTLA4). Combination therapy resulted with improved responses for these treatment models [14].

There is a non-negligible amount of evidence for acidic tumor microenvironment being responsible from progression, invasion and in particular; resistance to chemo and immuno -therapies [139].

Great progress has been made in the field of tumor immunology but response rates are still low which gives a clue that there are additional immunosuppressive pathways. Aside from cell-based inhibitors (such as regulatory T cells, myeloid derived suppressor cells) and secreted factors (such as kynurenines), there has been also strong evidence for tumor-derived acidity being responsible from immune suppression [14].

In a previous study, it was shown that oral bicarbonate therapy with checkpoint blockade achieved to increase tumor pH and improved immunotherapy responses [14]. As combinatorial approach of targeting tumor pH and immunotherapy has promising outcomes we proposed to investigate pharmacological interventions that will achieve neutralization of tumor acidosis and can be translated to clinic.

L-DOS47 is an urease conjugated antibody that targets human CEACAM6 antigen which is upregulated in several cancers including pancreatic and lung. L-DOS47 increases pH by converting urea to 2  $\text{NH}_4^+$  and 1  $\text{HCO}_3^-$ , producing a net local increase in pH. L-DOS47, is currently in clinical trials for the treatment of non squamous small cell lung cancer (NSCLC) and well tolerated. It is a strong candidate for being used in combination with immunotherapy in the near future.

First hypothesis of the thesis was developing methods to image tumor pH with MRI and/or MRS. This was accomplished with optimization and development of  $^{31}\text{P}$  MRS of 3-APP and CEST MRI methods in Small Animal Imaging Lab (SAIL) at Moffitt Cancer Center. Those methods have shown that L-DOS47 was effective on increase of tumor pH in vivo in two different CEACAM6 cancer models (BxPC3 human pancreatic and engineered Panc 02 murine pancreatic cells) for the first time. pH differences determined between control and L-DOS47 treated mice in 24 hours were significantly different based on t test ( $p < 0.05$ ). Particularly, CEST imaging with Isovuc has great potential to be translated to clinic since the contrast agent is already approved to be used for CT by FDA.

Besides pH measurement studies, the drug (urease) activity was shown with hyperpolarized MRS experiments. Those experiments clearly demonstrated the products

of conversion from urea to ammonia caused by urease. To our knowledge, this was the first HP-MRS experiment showed urease enzyme activity. However, it remains unclear whether the enzyme activity will be sufficiently high to observe in vivo.

In vivo experiments for immunotherapy combination treatment with L-DOS47 were designed. In the first experiment designed with Panc02 Clone 38 cells, with a small group of animals it was shown that L-DOS47 in combination with anti-PD1 treatment was effective on tumor growth. L-DOS47 and anti-PD1 alone each were similarly effective at partially reducing tumor growth. However, when L-DOS47 and anti-PD1 treatments were combined, a dramatic reduction in tumor growth was observed. It was encouraging to observe excellent combined activity of combination treatment. This result supports the observation that the therapy with sodium bicarb buffer improved PD-1 immunotherapy suggests that addition of L-DOS47 could be used to improve immunotherapy response as well.

In order to prove the concept three more in vivo experiments were designed with similar set-ups with increased number of mice in each group. In total 148 mice were included to overall experiments with mixed genders and they were sacrificed when they reached to endpoint according to Institutional Animal Care and Use Committee (IACUC) regulations. Kaplan Meier survival curves were generated in terms of including 37 mice/ group and it was shown that L-DOS47 treatment is effective to promote survival when combined with anti-PD1 (survivals were different than anti-PD1 alone  $p < 0.06$  and control groups  $p < 0.0001$ ).

According to our knowledge, it is the first time that proposed drug was tested for its capability to neutralize the tumor acidity with in-vivo models. In addition to that, we added peritumoral acidosis as an important and targetable immune modulator through pre-clinical trials. Knowledge of localized pH within tumors may allow more detailed information about tumor habitats, processes and relate them to intratumoral pH heterogeneity.

Personalized medicine treatment is becoming more and more important but can-

cer patients are still treated with a one-size-fits-all standard approach today. However as each person has their own fingerprint, they also have their unique cancer diseases. It is -most of the time- not possible to expect the same output with applying the same treatment to two different patients even if they have the exact same advanced cancer. They may respond completely different from each other as it is being commonly observed in the clinic. It is important tailor the treatment for each patient based on their cancer as unique signature to provide the maximum benefit while keeping the side effects minimum. For instance during MRI of tumor microenvironment experiments it was observed that tumors of some mice were not acidic (pH equal or greater than 7) which suggests having pH as an inclusion criteria for a potential clinical trial can contribute to the benefits of patients and help cancer professionals to make decisions based on that.

Overall, under the scope of this PhD work the methods developed to measure tumor pH and combinatorial approaches in order to improve immunotherapy responses have potential to be used in the clinic for patient benefits. Experiments with different cell lines are ongoing to have a robust treatment model. Same approach can be applied to mouse studies as including mice after having pH measurements to have better responses. MR imaging can be also combined with Position Emission Tomography (PET) in order to both measure pH and correlate this with functional imaging data. Increased glucose metabolism as an hallmark of cancer and its relation with acidosis will provide better understanding of tumor microenvironment [140].

## APPENDIX A. LIST OF PUBLICATIONS PRODUCED FROM THE THESIS

1. Damgaci, S., Ibrahim-Hashim, A., Enriquez-Navas, P.M., Pilon-Thomas, S., Guvenis, A. and Gillies, R.J., 2018. Hypoxia and acidosis: immune suppressors and therapeutic targets. *Immunology*, 154(3), pp.354-362.
2. Damgaci, S., Ibrahim-Hashim, A., Enriquez-Navas, P.M., Pilon-Thomas, S., Guvenis, A. and Gillies, R.J., 2019. Immunotherapy on Acid. *European Journal of Clinical Nutrition*, accepted.
3. Damgaci, S., Chao,H., Uger, M., Martinez, G., Enriquez-Navas, P.M., Longo, D., Abrahams, D., Ibrahim-Hashim, A., Dominguez Viqueira, W., Guvenis, A. and Gillies, R.J., 2020. Pharmacodynamics of targeted urease using CEST and 31P of 3-APP. *Magnetic Resonance Imaging*, to be submitted.
4. Damgaci, S., Chao,H., Uger,M., Enriquez-Navas, P., Abrahams, D., Ibrahim-Hashim, A., Guvenis, A. and Gillies, R.J., 2020. Targeting tumor pH with L-DOS47 to improve immunotherapy responses. *Cancer Research*, to be submitted.
5. Damgaci, S., Chao, H., Uger, MD., Ibrahim-Hashim, A., Kim, E., Enriquez-Navas P, Abrahams, D., Anderson, AR., Guvenis, A., Gillies, RJ. Improving survival in pancreatic cancer using Doxorubicin in combination with L-DOS47. *American Association for Cancer Research Annual Meeting (AACR 2019)*, Atlanta, U.S.
6. Damgaci, S., Chao,H., Uger, MD., Martinez, G., Enriquez-Navas, P.M., Longo, D., Abrahams, D., Ibrahim-Hashim, A., Dominguez Viqueira, W., Guvenis, A. and Gillies, R.J. MR Pharmacodynamics of targeted urease and checkpoint blockade using CEST and 31P MRSI. Is there a role for hyperpolarized 13C & 15N? *World Molecular Imaging Congress (WMIC 2019)*, Montreal, Canada.

## REFERENCES

1. Hanahan, D., and R. A. Weinberg, "Hallmarks of cancer: the next generation," *cell*, Vol. 144, no. 5, pp. 646–674, 2011.
2. Vaupel, P., F. Kallinowski, and P. Okunieff, "Blood flow, oxygen and nutrient supply, and metabolic microenvironment of human tumors: a review," *Cancer research*, Vol. 49, no. 23, pp. 6449–6465, 1989.
3. Cairns, R., I. Papandreou, and N. Denko, "Overcoming physiologic barriers to cancer treatment by molecularly targeting the tumor microenvironment," *Molecular Cancer Research*, Vol. 4, no. 2, pp. 61–70, 2006.
4. Gatenby, R. A., and R. J. Gillies, "Why do cancers have high aerobic glycolysis?," *Nature reviews cancer*, Vol. 4, no. 11, p. 891, 2004.
5. Warburg, O., "On the origin of cancer cells," *Science*, Vol. 123, no. 3191, pp. 309–314, 1956.
6. Justus, C. R., L. Dong, and L. V. Yang, "Acidic tumor microenvironment and ph-sensing g protein-coupled receptors," *Frontiers in physiology*, Vol. 4, p. 354, 2013.
7. Izumi, H., T. Torigoe, H. Ishiguchi, H. Uramoto, Y. Yoshida, M. Tanabe, T. Ise, T. Murakami, T. Yoshida, M. Nomoto, *et al.*, "Cellular ph regulators: potentially promising molecular targets for cancer chemotherapy," *Cancer treatment reviews*, Vol. 29, no. 6, pp. 541–549, 2003.
8. Boedtkjer, E., J. M. Moreira, M. Mele, P. Vahl, V. T. Wielenga, P. M. Christiansen, V. E. Jensen, S. F. Pedersen, and C. Aalkjaer, "Contribution of na<sup>+</sup>, hco<sub>3</sub><sup>-</sup>-cotransport to cellular ph control in human breast cancer: A role for the breast cancer susceptibility locus nbcn1 (slc4a7)," *International journal of cancer*, Vol. 132, no. 6, pp. 1288–1299, 2013.
9. Kellum, J., *et al.*, "Metabolic acidosis in patients with sepsis: epiphenomenon or part of the pathophysiology?," *Critical Care and Resuscitation*, Vol. 6, no. 3, p. 197, 2004.
10. Lardner, A., "The effects of extracellular ph on immune function," *Journal of leukocyte biology*, Vol. 69, no. 4, pp. 522–530, 2001.
11. Bellone, M., A. Calcinotto, P. Filipazzi, A. De Milito, S. Fais, and L. Rivoltini, "The acidity of the tumor microenvironment is a mechanism of immune escape that can be overcome by proton pump inhibitors," *Oncoimmunology*, Vol. 2, no. 1, p. e22058, 2013.
12. McDonald, P. C., S. C. Chafe, and S. Dedhar, "Overcoming hypoxia-mediated tumor progression: combinatorial approaches targeting ph regulation, angiogenesis and immune dysfunction," *Frontiers in cell and developmental biology*, Vol. 4, p. 27, 2016.
13. Dong, L., Z. Li, N. R. Leffler, A. S. Asch, J.-T. Chi, and L. V. Yang, "Acidosis activation of the proton-sensing gpr4 receptor stimulates vascular endothelial cell inflammatory responses revealed by transcriptome analysis," *PloS one*, Vol. 8, no. 4, p. e61991, 2013.
14. Pilon-Thomas, S., K. N. Kodumudi, A. E. El-Kenawi, S. Russell, A. M. Weber, K. Luddy, M. Damaghi, J. W. Wojtkowiak, J. J. Mulé, A. Ibrahim-Hashim, *et al.*, "Neutralization of tumor acidity improves antitumor responses to immunotherapy," *Cancer research*, Vol. 76, no. 6, pp. 1381–1390, 2016.

15. Anemone, A., L. Consolino, F. Arena, M. Capozza, and D. L. Longo, "Imaging tumor acidosis: a survey of the available techniques for mapping in vivo tumor ph," *Cancer and Metastasis Reviews*, pp. 1–25, 2019.
16. Damgaci, S., A. Ibrahim-Hashim, P. M. Enriquez-Navas, S. Pilon-Thomas, A. Guvenis, and R. J. Gillies, "Hypoxia and acidosis: immune suppressors and therapeutic targets," *Immunology*, Vol. 154, no. 3, pp. 354–362, 2018.
17. Li, H., X. Fan, and J. Houghton, "Tumor microenvironment: the role of the tumor stroma in cancer," *Journal of cellular biochemistry*, Vol. 101, no. 4, pp. 805–815, 2007.
18. Bremnes, R. M., K. Al-Shibli, T. Donnem, R. Sirera, S. Al-Saad, S. Andersen, H. Stenvold, C. Camps, and L.-T. Busund, "The role of tumor-infiltrating immune cells and chronic inflammation at the tumor site on cancer development, progression, and prognosis: emphasis on non-small cell lung cancer," *Journal of Thoracic Oncology*, Vol. 6, no. 4, pp. 824–833, 2011.
19. Hanahan, D., and L. M. Coussens, "Accessories to the crime: functions of cells recruited to the tumor microenvironment," *Cancer cell*, Vol. 21, no. 3, pp. 309–322, 2012.
20. Sica, A., and A. Mantovani, "Macrophage plasticity and polarization: in vivo veritas," *The Journal of clinical investigation*, Vol. 122, no. 3, pp. 787–795, 2012.
21. Vignali, D. A., L. W. Collison, and C. J. Workman, "How regulatory t cells work," *Nature Reviews Immunology*, Vol. 8, no. 7, p. 523, 2008.
22. Topalian, S. L., C. G. Drake, and D. M. Pardoll, "Targeting the pd-1/b7-h1 (pd-l1) pathway to activate anti-tumor immunity," *Current opinion in immunology*, Vol. 24, no. 2, pp. 207–212, 2012.
23. Draghiciu, O., H. W. Nijman, and T. Daemen, "From tumor immunosuppression to eradication: targeting homing and activity of immune effector cells to tumors," *Clinical and Developmental Immunology*, Vol. 2011, 2011.
24. Kryczek, I., L. Zou, P. Rodriguez, G. Zhu, S. Wei, P. Mottram, M. Brumlik, P. Cheng, T. Curiel, L. Myers, *et al.*, "B7-h4 expression identifies a novel suppressive macrophage population in human ovarian carcinoma," *Journal of Experimental Medicine*, Vol. 203, no. 4, pp. 871–881, 2006.
25. Diaz-Montero, C. M., J. Finke, and A. J. Montero, "Myeloid-derived suppressor cells in cancer: therapeutic, predictive, and prognostic implications," in *Seminars in oncology*, Vol. 41, pp. 174–184, Elsevier, 2014.
26. Carreau, A., B. E. Hafny-Rahbi, A. Matejuk, C. Grillon, and C. Kieda, "Why is the partial oxygen pressure of human tissues a crucial parameter? small molecules and hypoxia," *Journal of cellular and molecular medicine*, Vol. 15, no. 6, pp. 1239–1253, 2011.
27. Wigerup, C., S. Pählman, and D. Bexell, "Therapeutic targeting of hypoxia and hypoxia-inducible factors in cancer," *Pharmacology & therapeutics*, Vol. 164, pp. 152–169, 2016.
28. Gillies, R. J., P. A. Schomack, T. W. Secomb, and N. Raghunand, "Causes and effects of heterogeneous perfusion in tumors," *Neoplasia*, Vol. 1, no. 3, pp. 197–207, 1999.
29. Jain, R. K., "Normalization of tumor vasculature: an emerging concept in antiangiogenic therapy," *Science*, Vol. 307, no. 5706, pp. 58–62, 2005.



30. Palazón, A., J. Aragonés, A. Morales-Kastresana, M. O. de Landázuri, and I. Melero, “Molecular pathways: hypoxia response in immune cells fighting or promoting cancer,” *Clinical Cancer Research*, Vol. 18, no. 5, pp. 1207–1213, 2012.
31. Atkuri, K. R., L. A. Herzenberg, A.-K. Niemi, T. Cowan, and L. A. Herzenberg, “Importance of culturing primary lymphocytes at physiological oxygen levels,” *Proceedings of the National Academy of Sciences*, Vol. 104, no. 11, pp. 4547–4552, 2007.
32. Atkuri, K. R., L. A. Herzenberg, and L. A. Herzenberg, “Culturing at atmospheric oxygen levels impacts lymphocyte function,” *Proceedings of the National Academy of Sciences*, Vol. 102, no. 10, pp. 3756–3759, 2005.
33. Ohta, A., R. Diwanji, R. Kini, M. Subramanian, A. Ohta, and M. Sitkovsky, “In vivo t cell activation in lymphoid tissues is inhibited in the oxygen-poor microenvironment,” *Frontiers in immunology*, Vol. 2, p. 27, 2011.
34. Neumann, A. K., J. Yang, M. P. Biju, S. K. Joseph, R. S. Johnson, V. H. Haase, B. D. Freedman, and L. A. Turka, “Hypoxia inducible factor 1 $\alpha$  regulates t cell receptor signal transduction,” *Proceedings of the National Academy of Sciences*, Vol. 102, no. 47, pp. 17071–17076, 2005.
35. Clambey, E. T., E. N. McNamee, J. A. Westrich, L. E. Glover, E. L. Campbell, P. Jedlicka, E. F. de Zoeten, J. C. Cambier, K. R. Stenmark, S. P. Colgan, *et al.*, “Hypoxia-inducible factor-1 alpha-dependent induction of foxp3 drives regulatory t-cell abundance and function during inflammatory hypoxia of the mucosa,” *Proceedings of the National Academy of Sciences*, Vol. 109, no. 41, pp. E2784–E2793, 2012.
36. Hasmim, M., M. Z. Noman, Y. Messai, D. Bordereaux, G. Gros, V. Baud, and S. Chouaib, “Cutting edge: hypoxia-induced nanog favors the intratumoral infiltration of regulatory t cells and macrophages via direct regulation of tgf- $\beta$ 1,” *The Journal of Immunology*, Vol. 191, no. 12, pp. 5802–5806, 2013.
37. Facciabene, A., X. Peng, I. S. Hagemann, K. Balint, A. Barchetti, L.-P. Wang, P. A. Gimotty, C. B. Gilks, P. Lal, L. Zhang, *et al.*, “Tumour hypoxia promotes tolerance and angiogenesis via ccl28 and t reg cells,” *Nature*, Vol. 475, no. 7355, p. 226, 2011.
38. Yang, M., C. Ma, S. Liu, J. Sun, Q. Shao, W. Gao, Y. Zhang, Z. Li, Q. Xie, Z. Dong, *et al.*, “Hypoxia skews dendritic cells to a t helper type 2-stimulating phenotype and promotes tumour cell migration by dendritic cell-derived osteopontin,” *Immunology*, Vol. 128, no. 1pt2, pp. e237–e249, 2009.
39. Dang, E. V., J. Barbi, H.-Y. Yang, D. Jinasena, H. Yu, Y. Zheng, Z. Bordman, J. Fu, Y. Kim, H.-R. Yen, *et al.*, “Control of th17/treg balance by hypoxia-inducible factor 1,” *Cell*, Vol. 146, no. 5, pp. 772–784, 2011.
40. Ohta, A., E. Gorelik, S. J. Prasad, F. Ronchese, D. Lukashev, M. K. Wong, X. Huang, S. Caldwell, K. Liu, P. Smith, *et al.*, “A2a adenosine receptor protects tumors from antitumor t cells,” *Proceedings of the National Academy of Sciences*, Vol. 103, no. 35, pp. 13132–13137, 2006.
41. Caldwell, C. C., H. Kojima, D. Lukashev, J. Armstrong, M. Farber, S. G. Apasov, and M. V. Sitkovsky, “Differential effects of physiologically relevant hypoxic conditions on t lymphocyte development and effector functions,” *The Journal of Immunology*, Vol. 167, no. 11, pp. 6140–6149, 2001.

42. Thiel, M., C. C. Caldwell, S. Kreth, S. Kuboki, P. Chen, P. Smith, A. Ohta, A. B. Lentsch, D. Lukashev, and M. V. Sitkovsky, "Targeted deletion of hif-1 $\alpha$  gene in t cells prevents their inhibition in hypoxic inflamed tissues and improves septic mice survival," *PLoS One*, Vol. 2, no. 9, p. e853, 2007.
43. Noman, M. Z., G. Desantis, B. Janji, M. Hasmmim, S. Karray, P. Dessen, V. Bronte, and S. Chouaib, "Pd-11 is a novel direct target of hif-1 $\alpha$ , and its blockade under hypoxia enhanced mdsc-mediated t cell activation," *Journal of Experimental Medicine*, Vol. 211, no. 5, pp. 781–790, 2014.
44. Barsoum, I. B., T. K. Hamilton, X. Li, T. Cotechini, E. A. Miles, D. R. Siemens, and C. H. Graham, "Hypoxia induces escape from innate immunity in cancer cells via increased expression of adam10: role of nitric oxide," *Cancer research*, Vol. 71, no. 24, pp. 7433–7441, 2011.
45. Chouaib, S., M. Noman, K. Kosmatopoulos, and M. Curran, "Hypoxic stress: obstacles and opportunities for innovative immunotherapy of cancer," *Oncogene*, Vol. 36, no. 4, p. 439, 2017.
46. Labiano, S., A. Palazon, and I. Melero, "Immune response regulation in the tumor microenvironment by hypoxia," in *Seminars in oncology*, Vol. 42, pp. 378–386, Elsevier, 2015.
47. Berchem, G., M. Z. Noman, M. Bosseler, J. Paggetti, S. Baconnais, E. Le Cam, A. Nambakhsh, E. Moussay, F. Mami-Chouaib, B. Janji, *et al.*, "Hypoxic tumor-derived microvesicles negatively regulate nk cell function by a mechanism involving tgf- $\beta$  and mir23a transfer," *Oncoimmunology*, Vol. 5, no. 4, p. e1062968, 2016.
48. Baginska, J., E. Viry, G. Berchem, A. Poli, M. Z. Noman, K. van Moer, S. Medves, J. Zimmer, A. Oudin, S. P. Niclou, *et al.*, "Granzyme b degradation by autophagy decreases tumor cell susceptibility to natural killer-mediated lysis under hypoxia," *Proceedings of the National Academy of Sciences*, Vol. 110, no. 43, pp. 17450–17455, 2013.
49. Viry, E., J. Baginska, G. Berchem, M. Z. Noman, S. Medves, S. Chouaib, and B. Janji, "Autophagic degradation of gzmb/granzyme b: a new mechanism of hypoxic tumor cell escape from natural killer cell-mediated lysis," *Autophagy*, Vol. 10, no. 1, pp. 173–175, 2014.
50. Janji, B., E. Viry, E. Moussay, J. Paggetti, T. Arakelian, T. Mgrditchian, Y. Messai, M. Z. Noman, K. Van Moer, M. Hasmmim, *et al.*, "The multifaceted role of autophagy in tumor evasion from immune surveillance," *Oncotarget*, Vol. 7, no. 14, p. 17591, 2016.
51. Tittarelli, A., B. Janji, K. Van Moer, M. Z. Noman, and S. Chouaib, "The selective degradation of synaptic connexin 43 protein by hypoxia-induced autophagy impairs natural killer cell-mediated tumor cell killing," *Journal of Biological Chemistry*, Vol. 290, no. 39, pp. 23670–23679, 2015.
52. Sceneay, J., M. T. Chow, A. Chen, H. M. Halse, C. S. Wong, D. M. Andrews, E. K. Sloan, B. S. Parker, D. D. Bowtell, M. J. Smyth, *et al.*, "Primary tumor hypoxia recruits cd11b+/ly6med/ly6g+ immune suppressor cells and compromises nk cell cytotoxicity in the premetastatic niche," *Cancer research*, Vol. 72, no. 16, pp. 3906–3911, 2012.
53. Varol, C., A. Mildner, and S. Jung, "Macrophages: development and tissue specialization," *Annual review of immunology*, Vol. 33, pp. 643–675, 2015.

54. Lewis, C., and C. Murdoch, "Macrophage responses to hypoxia: implications for tumor progression and anti-cancer therapies," *The American journal of pathology*, Vol. 167, no. 3, pp. 627–635, 2005.
55. Lin, E. Y., J.-F. Li, L. Gnatovskiy, Y. Deng, L. Zhu, D. A. Grzesik, H. Qian, X.-n. Xue, and J. W. Pollard, "Macrophages regulate the angiogenic switch in a mouse model of breast cancer," *Cancer research*, Vol. 66, no. 23, pp. 11238–11246, 2006.
56. Qian, B.-Z., and J. W. Pollard, "Macrophage diversity enhances tumor progression and metastasis," *Cell*, Vol. 141, no. 1, pp. 39–51, 2010.
57. Murdoch, C., and C. E. Lewis, "Macrophage migration and gene expression in response to tumor hypoxia," *International journal of cancer*, Vol. 117, no. 5, pp. 701–708, 2005.
58. Wang, N., H. Liang, and K. Zen, "Molecular mechanisms that influence the macrophage m1–m2 polarization balance," *Frontiers in immunology*, Vol. 5, p. 614, 2014.
59. Movahedi, K., D. Laoui, C. Gysemans, M. Baeten, G. Stangé, J. Van den Bossche, M. Mack, D. Pipeleers, P. In't Veld, P. De Baetselier, *et al.*, "Different tumor microenvironments contain functionally distinct subsets of macrophages derived from ly6c (high) monocytes," *Cancer research*, Vol. 70, no. 14, pp. 5728–5739, 2010.
60. Fang, H.-Y., R. Hughes, C. Murdoch, S. B. Coffelt, S. K. Biswas, A. L. Harris, R. S. Johnson, H. Z. Imityaz, M. C. Simon, E. Fredlund, *et al.*, "Hypoxia-inducible factors 1 and 2 are important transcriptional effectors in primary macrophages experiencing hypoxia," *Blood*, Vol. 114, no. 4, pp. 844–859, 2009.
61. Peyssonnaud, C., V. Datta, T. Cramer, A. Doedens, E. A. Theodorakis, R. L. Gallo, N. Hurtado-Ziola, V. Nizet, and R. S. Johnson, "Hif-1 $\alpha$  expression regulates the bactericidal capacity of phagocytes," *The Journal of clinical investigation*, Vol. 115, no. 7, pp. 1806–1815, 2005.
62. Blouin, C. C., E. L. Pagé, G. M. Soucy, and D. E. Richard, "Hypoxic gene activation by lipopolysaccharide in macrophages: implication of hypoxia-inducible factor 1 $\alpha$ ," *Blood*, Vol. 103, no. 3, pp. 1124–1130, 2004.
63. Walmsley, S. R., N. Farahi, C. Peyssonnaud, R. S. Johnson, T. Cramer, A. Sobolewski, A. M. Condliffe, A. S. Cowburn, N. Johnson, E. R. Chilvers, *et al.*, "Hypoxia-induced neutrophil survival is mediated by hif-1 $\alpha$ -dependent nf- $\kappa$ b activity," *Journal of Experimental Medicine*, Vol. 201, no. 1, pp. 105–115, 2005.
64. Takeda, N., E. L. O'Dea, A. Doedens, J.-w. Kim, A. Weidemann, C. Stockmann, M. Asagiri, M. C. Simon, A. Hoffmann, and R. S. Johnson, "Differential activation and antagonistic function of hif- $\alpha$  isoforms in macrophages are essential for homeostasis," *Genes & development*, Vol. 24, no. 5, pp. 491–501, 2010.
65. Rodríguez-Prados, J.-C., P. G. Través, J. Cuenca, D. Rico, J. Aragonés, P. Martín-Sanz, M. Cascante, and L. Boscá, "Substrate fate in activated macrophages: a comparison between innate, classic, and alternative activation," *The Journal of Immunology*, Vol. 185, no. 1, pp. 605–614, 2010.
66. Bansal, V., and J. B. Ochoa, "Arginine availability, arginase, and the immune response," *Current Opinion in Clinical Nutrition & Metabolic Care*, Vol. 6, no. 2, pp. 223–228, 2003.

67. De Palma, M., M. A. Venneri, R. Galli, L. S. Sergi, L. S. Politi, M. Sampaolesi, and L. Naldini, "Tie2 identifies a hematopoietic lineage of proangiogenic monocytes required for tumor vessel formation and a mesenchymal population of pericyte progenitors," *Cancer cell*, Vol. 8, no. 3, pp. 211–226, 2005.
68. Doedens, A. L., C. Stockmann, M. P. Rubinstein, D. Liao, N. Zhang, D. G. DeNardo, L. M. Coussens, M. Karin, A. W. Goldrath, and R. S. Johnson, "Macrophage expression of hypoxia-inducible factor-1 $\alpha$  suppresses t-cell function and promotes tumor progression," *Cancer research*, Vol. 70, no. 19, pp. 7465–7475, 2010.
69. Bekes, E. M., B. Schweighofer, T. A. Kupriyanova, E. Zajac, V. C. Ardi, J. P. Quigley, and E. I. Deryugina, "Tumor-recruited neutrophils and neutrophil timp-free mmp-9 regulate coordinately the levels of tumor angiogenesis and efficiency of malignant cell intravasation," *The American journal of pathology*, Vol. 179, no. 3, pp. 1455–1470, 2011.
70. Walmsley, S. R., E. R. Chilvers, A. A. Thompson, K. Vaughan, H. M. Marriott, L. C. Parker, G. Shaw, S. Parmar, M. Schneider, I. Sabroe, *et al.*, "Prolyl hydroxylase 3 (phd3) is essential for hypoxic regulation of neutrophilic inflammation in humans and mice," *The Journal of clinical investigation*, Vol. 121, no. 3, pp. 1053–1063, 2011.
71. Hannah, S., K. Mecklenburgh, I. Rahman, G. J. Bellingan, A. Greening, C. Haslett, and E. R. Chilvers, "Hypoxia prolongs neutrophil survival in vitro," *FEBS letters*, Vol. 372, no. 2-3, pp. 233–237, 1995.
72. Rotstein, O. D., V. D. Fiegel, R. L. Simmons, and D. R. Knighton, "The deleterious effect of reduced ph and hypoxia on neutrophil migration in vitro," *Journal of Surgical Research*, Vol. 45, no. 3, pp. 298–303, 1988.
73. Jantsch, J., D. Chakravorty, N. Turza, A. T. Prechtel, B. Buchholz, R. G. Gerlach, M. Volke, J. Gläsner, C. Warnecke, M. S. Wiesener, *et al.*, "Hypoxia and hypoxia-inducible factor-1 $\alpha$  modulate lipopolysaccharide-induced dendritic cell activation and function," *The Journal of Immunology*, Vol. 180, no. 7, pp. 4697–4705, 2008.
74. Gillies, R. J., I. Robey, and R. A. Gatenby, "Causes and consequences of increased glucose metabolism of cancers," *Journal of Nuclear Medicine*, Vol. 49, no. 2, p. 24S, 2008.
75. Barbosa, I. A., N. G. Machado, A. J. Skildum, P. M. Scott, and P. J. Oliveira, "Mitochondrial remodeling in cancer metabolism and survival: potential for new therapies," *Biochimica et Biophysica Acta (BBA)-Reviews on Cancer*, Vol. 1826, no. 1, pp. 238–254, 2012.
76. Damaghi, M., N. K. Tafreshi, M. C. Lloyd, R. Sprung, V. Estrella, J. W. Wojtkowiak, D. L. Morse, J. M. Koomen, M. M. Bui, R. A. Gatenby, *et al.*, "Chronic acidosis in the tumour microenvironment selects for overexpression of lamp2 in the plasma membrane," *Nature communications*, Vol. 6, p. 8752, 2015.
77. Pardoll, D. M., "Immunology beats cancer: a blueprint for successful translation," *Nature immunology*, Vol. 13, no. 12, p. 1129, 2012.
78. Epstein, T., L. Xu, R. J. Gillies, and R. A. Gatenby, "Separation of metabolic supply and demand: aerobic glycolysis as a normal physiological response to fluctuating energetic demands in the membrane," *Cancer & metabolism*, Vol. 2, no. 1, p. 7, 2014.
79. Kareva, I., and P. Hahnfeldt, "The emerging hallmarks of metabolic reprogramming and immune evasion: distinct or linked?," *Cancer research*, Vol. 73, no. 9, pp. 2737–2742, 2013.

80. Hirschhaeuser, F., U. G. Sattler, and W. Mueller-Klieser, "Lactate: a metabolic key player in cancer," *Cancer research*, Vol. 71, no. 22, pp. 6921–6925, 2011.
81. Calcinotto, A., P. Filipazzi, M. Grioni, M. Iero, A. De Milito, A. Ricupito, A. Cova, R. Canese, E. Jachetti, M. Rossetti, *et al.*, "Modulation of microenvironment acidity reverses anergy in human and murine tumor-infiltrating t lymphocytes," *Cancer research*, Vol. 72, no. 11, pp. 2746–2756, 2012.
82. Demotte, N., V. Stroobant, P. J. Courtoy, P. Van Der Smissen, D. Colau, I. F. Luescher, C. Hivroz, J. Nicaise, J.-L. Squifflet, M. Mourad, *et al.*, "Restoring the association of the t cell receptor with cd8 reverses anergy in human tumor-infiltrating lymphocytes," *Immunity*, Vol. 28, no. 3, pp. 414–424, 2008.
83. Crowther, M., N. Brown, E. Bishop, and C. Lewis, "Microenvironmental influence on macrophage regulation of angiogenesis in wounds and malignant tumors," *Journal of leukocyte biology*, Vol. 70, no. 4, pp. 478–490, 2001.
84. Husain, Z., Y. Huang, P. Seth, and V. P. Sukhatme, "Tumor-derived lactate modifies antitumor immune response: effect on myeloid-derived suppressor cells and nk cells," *The Journal of Immunology*, Vol. 191, no. 3, pp. 1486–1495, 2013.
85. Bellocq, A., S. Suberville, C. Philippe, F. Bertrand, J. Perez, B. Fouqueray, G. Cherqui, and L. Baud, "Low environmental ph is responsible for the induction of nitric-oxide synthase in macrophages evidence for involvement of nuclear factor- $\kappa$ b activation," *Journal of Biological Chemistry*, Vol. 273, no. 9, pp. 5086–5092, 1998.
86. Colegio, O. R., N.-Q. Chu, A. L. Szabo, T. Chu, A. M. Rhebergen, V. Jairam, N. Cyrus, C. E. Brokowski, S. C. Eisenbarth, G. M. Phillips, *et al.*, "Functional polarization of tumour-associated macrophages by tumour-derived lactic acid," *Nature*, Vol. 513, no. 7519, p. 559, 2014.
87. El-Kenawi, A. E., A. A. Ibrahim-Hashim, K. A. Luddy, S. A. Pilon-Thomas, R. A. Gatenby, and R. J. Gillies, "Extracellular acidosis alters polarization of macrophages," 2015.
88. Trevani, A. S., G. Andonegui, M. Giordano, D. H. López, R. Gamberale, F. Minucci, and J. R. Geffner, "Extracellular acidification induces human neutrophil activation," *The Journal of Immunology*, Vol. 162, no. 8, pp. 4849–4857, 1999.
89. Martínez, D., M. Vermeulen, A. Trevani, A. Ceballos, J. Sabatté, R. Gamberale, M. E. Álvarez, G. Salamone, T. Tanos, O. A. Coso, *et al.*, "Extracellular acidosis induces neutrophil activation by a mechanism dependent on activation of phosphatidylinositol 3-kinase/akt and erk pathways," *The Journal of Immunology*, Vol. 176, no. 2, pp. 1163–1171, 2006.
90. Vermeulen, M., M. Giordano, A. S. Trevani, C. Sedlik, R. Gamberale, P. Fernández-Calotti, G. Salamone, S. Raiden, J. Sanjurjo, and J. R. Geffner, "Acidosis improves uptake of antigens and mhc class i-restricted presentation by dendritic cells," *The Journal of Immunology*, Vol. 172, no. 5, pp. 3196–3204, 2004.
91. Lazarus, D., C. Peters, A. Stockmann, S. Eliasof, and L. Jayaraman, "Crlx101, an investigational nanoparticle-drug conjugate of camptothecin, demonstrates synergy with immunotherapy agents in preclinical models," 2016.

92. Kheshtchin, N., S. Arab, M. Ajami, R. Mirzaei, M. Ashourpour, N. Mousavi, N. Khosravianfar, F. Jadidi-Niaragh, A. Namdar, F. Noorbakhsh, *et al.*, “Inhibition of hif-1 $\alpha$  enhances anti-tumor effects of dendritic cell-based vaccination in a mouse model of breast cancer,” *Cancer Immunology, Immunotherapy*, Vol. 65, no. 10, pp. 1159–1167, 2016.
93. Noman, M. Z., M. Hasmmim, Y. Messai, S. Terry, C. Kieda, B. Janji, and S. Chouaib, “Hypoxia: a key player in antitumor immune response. a review in the theme: cellular responses to hypoxia,” *American Journal of Physiology-Cell Physiology*, Vol. 309, no. 9, pp. C569–C579, 2015.
94. Ai, M., P. Budhani, J. Sheng, S. Balasubramanyam, T. Bartkowiak, A. R. Jaiswal, C. R. Ager, D. D. Haria, and M. A. Curran, “Tumor hypoxia drives immune suppression and immunotherapy resistance,” *Journal for immunotherapy of cancer*, Vol. 3, no. S2, p. P392, 2015.
95. Portwood, S., D. Lal, Y.-C. Hsu, R. Vargas, M. K. Johnson, M. Wetzler, C. P. Hart, and E. S. Wang, “Activity of the hypoxia-activated prodrug, th-302, in preclinical human acute myeloid leukemia models,” *Clinical Cancer Research*, Vol. 19, no. 23, pp. 6506–6519, 2013.
96. Hu, J., D. R. Handisides, E. Van Valckenborgh, H. De Raeve, E. Menu, I. V. Broek, Q. Liu, J. D. Sun, B. Van Camp, C. P. Hart, *et al.*, “Targeting the multiple myeloma hypoxic niche with th-302, a hypoxia-activated prodrug,” *Blood*, Vol. 116, no. 9, pp. 1524–1527, 2010.
97. Hashim, A. I., H. H. Cornnell, M. d. L. C. Ribeiro, D. Abrahams, J. Cunningham, M. Lloyd, G. V. Martinez, R. A. Gatenby, and R. J. Gillies, “Reduction of metastasis using a non-volatile buffer,” *Clinical & experimental metastasis*, Vol. 28, no. 8, pp. 841–849, 2011.
98. Ibrahim-Hashim, A., H. H. Cornnell, D. Abrahams, M. Lloyd, M. Bui, R. J. Gillies, and R. A. Gatenby, “Systemic buffers inhibit carcinogenesis in tramp mice,” *The Journal of urology*, Vol. 188, no. 2, pp. 624–631, 2012.
99. Ibrahim-Hashim, A., J. W. Wojtkowiak, M. d. L. C. Ribeiro, V. Estrella, K. M. Bailey, H. H. Cornnell, R. A. Gatenby, and R. J. Gillies, “Free base lysine increases survival and reduces metastasis in prostate cancer model,” *Journal of cancer science & therapy*, no. 4, 2011.
100. Robey, I. F., B. K. Baggett, N. D. Kirkpatrick, D. J. Roe, J. Doseescu, B. F. Sloane, A. I. Hashim, D. L. Morse, N. Raghunand, R. A. Gatenby, *et al.*, “Bicarbonate increases tumor ph and inhibits spontaneous metastases,” *Cancer research*, Vol. 69, no. 6, pp. 2260–2268, 2009.
101. Wong, W. Y., C. I. DeLuca, B. Tian, I. Wilson, S. Molund, N. Warriar, M. V. Govindan, D. Segal, and H. Chao, “Urease-induced alkalization of extracellular ph and its antitumor activity in human breast and lung cancers.” *Journal of experimental therapeutics & oncology*, Vol. 5, no. 2, 2005.
102. Tian, B., W. Y. Wong, E. Hegmann, K. Gaspar, P. Kumar, and H. Chao, “Production and characterization of a camelid single domain antibody–urease enzyme conjugate for the treatment of cancer,” *Bioconjugate chemistry*, Vol. 26, no. 6, pp. 1144–1155, 2015.
103. Zhang, Y., and J.-M. Yang, “Altered energy metabolism in cancer: a unique opportunity for therapeutic intervention,” *Cancer biology & therapy*, Vol. 14, no. 2, pp. 81–89, 2013.

104. Sonveaux, P., F. Végran, T. Schroeder, M. C. Wergin, J. Verrax, Z. N. Rabbani, C. J. De Saedeleer, K. M. Kennedy, C. Diepart, B. F. Jordan, *et al.*, “Targeting lactate-fueled respiration selectively kills hypoxic tumor cells in mice,” *The Journal of clinical investigation*, Vol. 118, no. 12, pp. 3930–3942, 2008.
105. Doherty, J. R., and J. L. Cleveland, “Targeting lactate metabolism for cancer therapeutics,” *The Journal of clinical investigation*, Vol. 123, no. 9, pp. 3685–3692, 2013.
106. Rajeshkumar, N., P. Dutta, S. Yabuuchi, R. F. De Wilde, G. V. Martinez, A. Le, J. J. Kamphorst, J. D. Rabinowitz, S. K. Jain, M. Hidalgo, *et al.*, “Therapeutic targeting of the warburg effect in pancreatic cancer relies on an absence of p53 function,” *Cancer research*, Vol. 75, no. 16, pp. 3355–3364, 2015.
107. Dutta, P., A. Le, D. L. Vander Jagt, T. Tsukamoto, G. V. Martinez, C. V. Dang, and R. J. Gillies, “Evaluation of ldh-a and glutaminase inhibition in vivo by hyperpolarized <sup>13</sup>c-pyruvate magnetic resonance spectroscopy of tumors,” *Cancer research*, Vol. 73, no. 14, pp. 4190–4195, 2013.
108. Buck, M. D., R. T. Sowell, S. M. Kaech, and E. L. Pearce, “Metabolic instruction of immunity,” *Cell*, Vol. 169, no. 4, pp. 570–586, 2017.
109. Gillies, R., Z. Liu, and Z. Bhujwala, “<sup>31</sup>p-mrs measurements of extracellular ph of tumors using 3-aminopropylphosphonate,” *American Journal of Physiology-Cell Physiology*, Vol. 267, no. 1, pp. C195–C203, 1994.
110. Van Sluis, R., Z. M. Bhujwala, N. Raghunand, P. Ballesteros, J. Alvarez, S. Cerdán, J.-P. Galons, and R. J. Gillies, “In vivo imaging of extracellular ph using <sup>1</sup>h mrsi,” *Magnetic Resonance in Medicine: An Official Journal of the International Society for Magnetic Resonance in Medicine*, Vol. 41, no. 4, pp. 743–750, 1999.
111. Pilot, C., A. Mahipal, and R. Gillies, “Buffer therapy—buffer diet,” *J. Nutr. Food Sci*, Vol. 8, 2018.
112. Blumenthal, R. D., E. Leon, H. J. Hansen, and D. M. Goldenberg, “Expression patterns of ceacam5 and ceacam6 in primary and metastatic cancers,” *BMC cancer*, Vol. 7, no. 1, p. 2, 2007.
113. Enriquez-Navas, P. M., and R. J. Gillies, “Measuring phi and phe by mrs,” *Emagres*, pp. 643–650, 2007.
114. Chaumeil, M. M., C. Najac, and S. M. Ronen, “Studies of metabolism using <sup>13</sup>c mrs of hyperpolarized probes,” in *Methods in enzymology*, Vol. 561, pp. 1–71, Elsevier, 2015.
115. Cho, A., J. Y. Lau, B. J. Geraghty, C. H. Cunningham, and K. R. Keshari, “Noninvasive interrogation of cancer metabolism with hyperpolarized <sup>13</sup>c mri,” *Journal of Nuclear Medicine*, Vol. 58, no. 8, pp. 1201–1206, 2017.
116. Kettunen, M. I., “Hyperpolarized mri for studying tumor metabolism,” in *Cancer Metabolism*, pp. 409–426, Springer, 2019.
117. Hundshammer, C., *Multimodal and Non-Invasive Imaging Techniques for a Multiparametric Characterization of Tumor Biology*. PhD thesis, Technische Universität München, 2019.

118. Stubbs, M., Z. M. Bhujwalla, G. Tozer, L. Rodrigues, R. Maxwell, R. Morgan, F. Howe, and J. Griffiths, "An assessment of  $^{31}\text{P}$  mrs as a method of measuring ph in rat tumours," *NMR in biomedicine*, Vol. 5, no. 6, pp. 351–359, 1992.
119. Soto, G. E., Z. Zhu, J. L. Evelhoch, and J. J. Ackerman, "Tumor  $^{31}\text{P}$  nmr ph measurements in vivo: a comparison of inorganic phosphate and intracellular 2-deoxyglucose-6-phosphate as phnmr indicators in murine radiation-induced fibrosarcoma-1," *Magnetic resonance in medicine*, Vol. 36, no. 5, pp. 698–704, 1996.
120. Lutz, N. W., Y. Le Fur, J. Chiche, J. Pouysségur, and P. J. Cozzone, "Quantitative in vivo characterization of intracellular and extracellular ph profiles in heterogeneous tumors: a novel method enabling multiparametric ph analysis," *Cancer research*, Vol. 73, no. 15, pp. 4616–4628, 2013.
121. Gerweck, L. E., and K. Seetharaman, "Cellular ph gradient in tumor versus normal tissue: potential exploitation for the treatment of cancer," *Cancer research*, Vol. 56, no. 6, pp. 1194–1198, 1996.
122. Longo, D. L., W. Dastrù, G. Digilio, J. Keupp, S. Langereis, S. Lanzardo, S. Prestigio, O. Steinbach, E. Terreno, F. Uggeri, *et al.*, "Iopamidol as a responsive mri-chemical exchange saturation transfer contrast agent for ph mapping of kidneys: in vivo studies in mice at 7 t," *Magnetic resonance in medicine*, Vol. 65, no. 1, pp. 202–211, 2011.
123. Aime, S., L. Calabi, L. Biondi, M. De Miranda, S. Ghelli, L. Paleari, C. Rebaudengo, and E. Terreno, "Iopamidol: exploring the potential use of a well-established x-ray contrast agent for mri," *Magnetic Resonance in Medicine: An Official Journal of the International Society for Magnetic Resonance in Medicine*, Vol. 53, no. 4, pp. 830–834, 2005.
124. Sun, P. Z., D. L. Longo, W. Hu, G. Xiao, and R. Wu, "Quantification of iopamidol multi-site chemical exchange properties for ratiometric chemical exchange saturation transfer (cest) imaging of ph," *Physics in Medicine & Biology*, Vol. 59, no. 16, p. 4493, 2014.
125. Ibrahim-Hashim, A., R. J. Gillies, J. S. Brown, and R. A. Gatenby, "Coevolution of tumor cells and their microenvironment: niche construction in cancer," in *Ecology and Evolution of Cancer*, pp. 111–117, Elsevier, 2017.
126. Yan, L., Y. Wang, Z.-Z. Wang, Y.-T. Rong, L.-L. Chen, Q. Li, T. Liu, Y.-H. Chen, Y.-D. Li, Z.-H. Huang, *et al.*, "Cell motility and spreading promoted by ceacam6 through cyclin d1/cdk4 in human pancreatic carcinoma," *Oncology reports*, Vol. 35, no. 1, pp. 418–426, 2016.
127. Gillies, R. J., C. Pilot, Y. Marunaka, and S. Fais, "Targeting acidity in cancer and diabetes," *Biochimica et Biophysica Acta (BBA)-Reviews on Cancer*, 2019.
128. Ribas, A., and J. D. Wolchok, "Cancer immunotherapy using checkpoint blockade," *Science*, Vol. 359, no. 6382, pp. 1350–1355, 2018.
129. Gong, J., A. Chehrazi-Raffle, S. Reddi, and R. Salgia, "Development of pd-1 and pd-11 inhibitors as a form of cancer immunotherapy: a comprehensive review of registration trials and future considerations," *Journal for immunotherapy of cancer*, Vol. 6, no. 1, p. 8, 2018.
130. Taube, J. M., A. Klein, J. R. Brahmer, H. Xu, X. Pan, J. H. Kim, L. Chen, D. M. Pardoll, S. L. Topalian, and R. A. Anders, "Association of pd-1, pd-1 ligands, and other features of the tumor immune microenvironment with response to anti-pd-1 therapy," *Clinical cancer research*, Vol. 20, no. 19, pp. 5064–5074, 2014.



131. Schneider, H., J. Downey, A. Smith, B. H. Zinselmeyer, C. Rush, J. M. Brewer, B. Wei, N. Hogg, P. Garside, and C. E. Rudd, "Reversal of the tcr stop signal by ctla-4," *science*, Vol. 313, no. 5795, pp. 1972–1975, 2006.
132. Hodi, F. S., S. J. O'Day, D. F. McDermott, R. W. Weber, J. A. Sosman, J. B. Haanen, R. Gonzalez, C. Robert, D. Schadendorf, J. C. Hassel, *et al.*, "Improved survival with ipilimumab in patients with metastatic melanoma," *New England Journal of Medicine*, Vol. 363, no. 8, pp. 711–723, 2010.
133. Topalian, S. L., M. Sznol, D. F. McDermott, H. M. Kluger, R. D. Carvajal, W. H. Sharfman, J. R. Brahmer, D. P. Lawrence, M. B. Atkins, J. D. Powderly, *et al.*, "Survival, durable tumor remission, and long-term safety in patients with advanced melanoma receiving nivolumab," *Journal of clinical oncology*, Vol. 32, no. 10, p. 1020, 2014.
134. Topalian, S. L., F. S. Hodi, J. R. Brahmer, S. N. Gettinger, D. C. Smith, D. F. McDermott, J. D. Powderly, R. D. Carvajal, J. A. Sosman, M. B. Atkins, *et al.*, "Safety, activity, and immune correlates of anti-pd-1 antibody in cancer," *New England Journal of Medicine*, Vol. 366, no. 26, pp. 2443–2454, 2012.
135. Wolchok, J. D., H. Kluger, M. K. Callahan, M. A. Postow, N. A. Rizvi, A. M. Lesokhin, N. H. Segal, C. E. Ariyan, R.-A. Gordon, K. Reed, *et al.*, "Nivolumab plus ipilimumab in advanced melanoma," *New England Journal of Medicine*, Vol. 369, no. 2, pp. 122–133, 2013.
136. Chan, C. H., and C. P. Stanners, "Novel mouse model for carcinoembryonic antigen-based therapy," *Molecular Therapy*, Vol. 9, no. 6, pp. 775–785, 2004.
137. Stratton, M. R., P. J. Campbell, and P. A. Futreal, "The cancer genome," *Nature*, Vol. 458, no. 7239, p. 719, 2009.
138. Warburg, O., F. Wind, and E. Negelein, "The metabolism of tumors in the body," *The Journal of general physiology*, Vol. 8, no. 6, p. 519, 1927.
139. Taylor, S., E. P. Spugnini, Y. G. Assaraf, T. Azzarito, C. Rauch, and S. Fais, "Microenvironment acidity as a major determinant of tumor chemoresistance: proton pump inhibitors (ppis) as a novel therapeutic approach," *Drug Resistance Updates*, Vol. 23, pp. 69–78, 2015.
140. Longo, D. L., A. Bartoli, L. Consolino, P. Bardini, F. Arena, M. Schwaiger, and S. Aime, "In vivo imaging of tumor metabolism and acidosis by combining pet and mri-cest ph imaging," *Cancer research*, Vol. 76, no. 22, pp. 6463–6470, 2016.